Residues at the interface between zinc binding and winged helix domains of human RECQ1 play a significant role in DNA strand annealing activity

Swagata Mukhopadhyay[1], Tulika Das[1], Madhuparna Bose[1], Chetan Kumar Jain[1], Mayukh Chakraborty[1], Sunandan Mukherjee [1,2], Kumari Shikha[3], Amit K. Das[1] and Agneyo Ganguly [1,*]

[1]Department of Biotechnology, Indian Institute of Technology Kharagpur, India, [2]International Institute of Molecular and Cell Biology in Warsaw, Poland and [3]School of Bioscience, Indian Institute of Technology Kharagpur, India

ABSTRACT

RECQ1 is the shortest among the five human RecQ helicases comprising of two RecA like domains, a zinc-binding domain and a RecQ C-terminal domain containing the winged-helix (WH). Mutations or deletions on the tip of a β-hairpin located in the WH domain are known to abolish the unwinding activity. Interestingly, the same mutations on the β-hairpin of annealing incompetent RECQ1 mutant (RECQ1[T1]) have been reported to restore its annealing activity. In an attempt to unravel the strand annealing mechanism, we have crystallized a fragment of RECQ1 encompassing D2–Zn–WH domains harbouring mutations on the β-hairpin. From our crystal structure data and interface analysis, we have demonstrated that an α-helix located in zinc-binding domain potentially interacts with residues of WH domain, which plays a significant role in strand annealing activity. We have shown that deletion of the α-helix or mutation of specific residues on it restores strand annealing activity of annealing deficient constructs of RECQ1. Our results also demonstrate that mutations on the α-helix induce conformational changes and affects DNA stimulated ATP hydrolysis and unwinding activity of RECQ1. Our study, for the first time, provides insight into the conformational requirements of the WH domain for efficient strand annealing by human RECQ1.

INTRODUCTION

RecQ helicases are highly conserved enzymes involved in vital cellular transactions like replication, transcription, repair and genome maintenance (1–3). These are 3′-5′ helicases that unwind a wide variety of DNA substrates and repair intermediates like forked duplex, Holliday junctions, D-loops and G-quadruplex DNA. In human, there are five RecQ helicases, of which RECQ1 is the shortest and the first one to be identified (4,5). Among the five RecQ helicases, BLM, WRN and RECQ4 have been linked to genetic disorders like Bloom Syndrome, Werner's syndrome and Rothmund-Thomson syndrome respectively (1–3). Although RECQ1 is not directly linked to any disease, it is known to be critical for maintaining genome stability (2,3). Moreover, increased susceptibility to breast cancer has also been reported for 'loss of function' mutations in RECQ1 (6–9). RECQ1 has been shown to play a significant role in replication fork restoration following repair of camptothecin induced DNA damage and fork stalling (10).

RECQ1 comprises 649 amino acids containing two signature RecA folds (D1 and D2), a zinc-binding domain (ZND) and a winged-helix (WH) domain. Human RECQ1 shares considerable structural similarity with *Escherichia coli* RecQ helicase (11,12). The *E. coli* RecQ and human RECQ1 differs prominently in the orientation of their WH domains relative to the helicase domains, as observed from their crystal structures (11,12). Depending on its oligomeric states, RECQ1 can efficiently unwind substrates like forked duplex, 3′ tailed duplex, Holliday junctions and three-stranded D-loops having a 3′ tail (13,14). Crystal structures of a near full-length RECQ1 (RECQ1[T1]: residues 49–616) in complex with ATPγS or with 3′ tailed duplex DNA clearly depicts the presence of a prominent β-hairpin structure in the WH domain. Mutations or deletion of residues on the β-hairpin leads to a severe loss of unwinding function (11,15,16). The β-hairpin was also shown to be involved in dimer formation (16). Like many other RecQ helicases, RECQ1 possesses ATP independent strand annealing activity, although the physiological role

---

of such activity is not very well studied (17,18). The *in vivo* role of strand annealing activity of RecQ helicases remain poorly understood. Strand annealing activity of BLM is thought to facilitate the formation and resolution of chicken foot structures, and is also required for double Holliday Junction resolution, thereby implicating significant roles in DNA repair and recombination (18–20). Sharma *et al*. suggested that RECQ1 might be involved in synthesis-dependent strand annealing (SDSA) where multiple unwinding and annealing cycles are required (17). The strand annealing activity of human RECQ1 has been extensively studied, although no clear mechanism could be proposed. Muzzolini *et al*. demonstrated that the higher-order oligomers of RECQ1 are associated with strand annealing while lower-order oligomers are responsible for unwinding (14). Recently some interesting findings reported by Pike *et al.*, including a crystal structure of the near full-length RECQ1 in complex with ssDNA, have provided some insight into the strand annealing mechanism. Pike *et al*. reported that the near full-length RECQ1 (RECQ1[T1]) retains unwinding capability but lacks annealing activity completely (11). Mutations on the β-hairpin in RECQ1[T1] (Δ2Y564A) led to a loss of unwinding but a gain in annealing activity (11,16). In the same paper, Pike *et al.* demonstrated that the isolated WH domain is capable of performing strand annealing, while a slightly bigger fragment comprising of D2, Zn and WH domains (D2–Zn–WH) completely lacks the annealing activity (15). Moreover, near full-length RECQ1 (RECQ1[T1]) crystallized with ssDNA exhibited the formation of a pseudoduplex stabilized by interactions with the WH domain (15). While the isolated WH domain can promote strand annealing similar to the full-length enzyme, RECQ1[T1] and D2–Zn–WH completely lack the annealing activity. Therefore, it may be hypothesized that the WH domain can shuttle between annealing competent and annealing incompetent conformations. A careful dissection of these findings justifies the necessity to revisit the mechanism of strand annealing and investigate the conformational requirement of the WH domain in DNA strand annealing activity.

In the present study, we have shown that mutations on the β-hairpin can restore strand annealing function of the truncated protein D2–Zn–WH. We crystallized the protein fragment D2–Zn–WH harbouring β-hairpin mutations (Δ2Y564A) and identified significant interactions between the Zn domain and WH domain that are disrupted due to these mutations. From the analysis of interface between the Zn and WH domains, we identified interacting residues on both the domains. Residues on the α-helix (420–430) located in the Zn domain have significant interactions with residues on the WH domain. Deletion of this α-helix or mutation of specific residues on it promotes strand annealing of D2–Zn–WH and RECQ1[T1]. The mutations on the β-hairpin or the α-helix were also found to severely affect the DNA binding of RECQ1 fragments. Collectively, our data for the first time provide evidence that interaction between WH and Zn domain restricts the WH domain in annealing incompetent conformation, and disruption of these interactions allow conformational changes that favour strand annealing.

MATERIALS AND METHODS

Cloning and site-directed mutagenesis

The sequence corresponding to the human RECQ1 truncated constructs, RECQ1[T1] (amino acid 49–616), D2–Zn–WH (amino acid 282–616), D2-Zn-CT (amino acid 282–649) and WH (amino acid 481–616), were amplified from the cDNA clone of human RECQ1 (Origene Technologies) using gene-specific primers (Supplementary Table S1). The fragments were cloned into pET28a vector at *Nde*I and *Bam*HI sites and transformed into *E. coli* DH5α cells. The deletion mutant D2–Zn–WH[Δhelix] was generated using overlap extension PCR. The construct comprises amino acids 282–616, lacking 10 residues (420–430) in the Zn-binding domain. All the clones were confirmed by sequencing.

The construct RECQ1[T1,helix4A] (containing four mutations F420A, F424A, S427A and S428A) was generated by PCR based mutagenesis using RECQ1[T1] (in pET28a) as template and mutagenic primers (listed in Supplementary Table S1). The constructs D2–Zn–WH[Δ2Y564A] and D2–Zn–WH[helix4A] were generated using mutagenic primers (listed in Supplementary Table S1) and D2–Zn–WH (in pET 28a) as a template. All amplifications were done using *Pfu* Ultra II Fusion HS polymerase (Agilent Technologies) and digested overnight with *Dpn*I (New England Biolabs) and transformed into *E. coli* DH5α competent cells. All the mutants were verified by sequencing.

Recombinant baculovirus expressing RECQ1[FL] or RECQ1[FLhelix4A] were generated using Baculodirect™expression System from Invitrogen. The full-length human RECQ1 ORF (corresponding to amino acid 1–649) was amplified using the cDNA clone of RECQ1 as a template and inserted into the pENTR3C vector between *Bam*HI and *Xho*I sites. The mutant construct RECQ1[FLhelix4A] was generated by PCR based mutagenesis using RECQ1 cloned in pENTR 3C vector as a template and mutagenic primers (listed in Supplementary Table S1). Recombinant baculovirus DNA was generated by an *in vitro* LR recombination reaction using the entry clone (in pENTR3C) and baculodirect linear DNA following the manufacturer's protocol. Sf9 cells were transfected with recombinant DNA harbouring RECQ1[FL] or RECQ1[FLhelix4A] using Cellfectin™ reagent. Following transfection, cells were incubated at 27°C for 72 h, and the virus was harvested from the culture medium after signs of infection appeared. The presence of the gene of interest within the baculovirus DNA was confirmed using PCR with gene-specific primers.

The sequence corresponding to a C-terminal deletion mutant of human RPA70 (RPA70[ΔC]) comprising amino acids 1–441 was PCR amplified from a cDNA clone of human RPA (Origene Technologies) using gene-specific primers. The gene fragment was cloned into pET28a vector at *Eco*RI and *Not*I sites and transformed into *E. coli* DH5α cells. The clone was confirmed by sequencing.

Overexpression and purification of RECQ1 constructs

Escherichia coli Rosetta (DE3) cells expressing constructs D2–Zn–WH, D2–Zn–WH[Δ2Y564A], D2-Zn-CT and

D2-Zn-CT$^{\Delta 2Y564A}$ were grown in Luria Bertani broth containing 50 μg/ml of Kanamycin and 34 μg/ml Chloramphenicol. The cells were grown up to OD$_{600}$ corresponding to 0.6 and induced with 1 mM isopropyl 1-thio-β-D-galactopyranoside (IPTG) at 22°C for 6 h at 150 rpm. *E. coli* Rosetta (DE3) expressing constructs isolated WH, WH$^{\Delta 2Y564A}$, D2–Zn–WH$^{\Delta helix}$ and D2–Zn–WH^{helix4A} were grown under similar conditions and were induced with 1 mM IPTG at 18°C for 6 h at 150 rpm. *E. coli* Rosetta (DE3) cells expressing RECQ1^{T1} and its mutant RECQ1$^{T1, helix4A}$ were grown in Terrific Broth up to OD$_{600}$ corresponding to 0.6 and induced with 0.5 mM IPTG at 22°C for 6 h at 150 rpm.

All the constructs mentioned above were purified using the following protocol. The cell pellets obtained after induction were resuspended in Buffer A (50 mM Tris–HCl (pH 7.5), 500 mM NaCl, 10 mM MgCl$_2$ and 1 mM β-ME) containing 10 mM Imidazole and 1mM Phenylmethylsulphonyl fluoride (PMSF). The cells were subjected to ultrasonicaton followed by centrifugation at 15 000g for 40 min. Nucleic acids and DNA-protein complexes were precipitated by adding 0.15% polyethyleneimine (pH 7.5) followed by centrifugation at 15 000g for 30 min at 4°C. The supernatant was loaded on to HisTrap FF Crude Ni-NTA column (GE healthcare). The column was washed with Buffer A containing 40 mM Imidazole. The proteins were eluted with Buffer A containing 100 mM Imidazole. The eluted fractions were collected and further subjected to size exclusion chromatography. Isolated WH and WH$^{\Delta 2Y564A}$ were further purified using S-75 column (16/600 Hi Load pg, GE Healthcare) equilibrated with Buffer A. For the rest of the constructs (D2–Zn–WH, D2–Zn–WH$^{\Delta 2Y564A}$, D2-Zn-CT, D2-Zn-CT$^{\Delta 2Y564A}$, D2–Zn–WH$^{\Delta helix}$, D2–Zn–WH^{helix4A}, RECQ1^{T1} and RECQ1^{T1,helix4A}), size exclusion chromatography was carried out using S-200 column (16/600 HiLoad pg, GE Healthcare) equilibrated with Buffer A. All purification steps were carried out at 4°C using ÄKTA-Prime Plus FPLC system (GE healthcare). The fractions containing the protein were analysed on a 12% SDS PAGE and were concentrated and flash-frozen in liquid nitrogen and stored at -80°C for further use.

For expression of full-length RECQ1^{FL} (649 aa) and its mutant (RECQ1^{FLhelix4A}), recombinant baculovirus particles were harvested after transfection and were used to infect fresh Sf9 cells. High titre viral stocks were generated, and plaque-forming units (pfu)/ml of the viral stock was determined using viral plaque assay. This high titre stock was used to infect fresh Sf9 cells at an MOI of 5 to produce recombinant RECQ1^{FL} or the mutant RECQ1^{FLhelix4A}. After 72 h of infection, the infected cells were harvested by centrifugation and resuspended in lysis buffer containing 50 mM Tris–HCl (pH 7.5), 500 mM NaCl, 1 mM β-ME, 5 mM Imidazole, 0.1% Triton X-100 and 1 mM phenylmethylsulphonyl fluoride (PMSF). The cells were subjected to ultrasonication followed by centrifugation at 15 000g for 30 min. Recombinant RECQ1^{FL} and RECQ1^{FLhelix4A} were purified using Ni-NTA affinity chromatography. The supernatant obtained after sonication and centrifugation was loaded onto Ni-NTA column equilibrated with Buffer A containing 5 mM Imidazole. The resin was washed

with Buffer A containing 30 mM Imidazole. The histidine-tagged RECQ1^{FL} was finally eluted using Buffer A containing 150 mM Imidazole. The mutant RECQ1^{FLhelix4A} was eluted with buffer A containing 200 mM Imidazole. The fractions containing the RECQ1 protein or its mutant was analysed on a 12% SDS PAGE. The proteins were buffer exchanged to buffer A, concentrated using Amicon Ultra centrifugal filters (Merck, Millipore), flash-frozen in liquid nitrogen and stored at -80°C for further use.

Escherichia coli Rosetta (DE3) expressing C-terminal deletion mutant of RPA70 (RPA70$^{\Delta C}$) were grown in Luria Bertani broth containing 50 μg/ml of Kanamycin and 34 μg/ml Chloramphenicol. The cells were grown up to OD$_{600}$ corresponding to 0.6 and induced with 0.5 mM IPTG at 37°C for 4 h at 150 rpm. The construct was purified using the following protocol. The cell pellets obtained after induction were resuspended in Buffer A containing 10 mM Imidazole and 1 mM PMSF. The cells were subjected to ultrasonicaton followed by centrifugation at 15 000g for 40 min. Nucleic acids and DNA-protein complexes were precipitated by adding 0.15% polyethyleneimine (pH 7.5) followed by centrifugation at 15 000g for 30 min at 4°C. The supernatant was loaded on to HisTrap FF Crude Ni-NTA column (GE healthcare). The column was washed with Buffer A containing 40 mM imidazole, and the protein was eluted with Buffer A containing 100 mM imidazole. The eluted fractions were collected and further subjected to size exclusion chromatography using S-200 column (16/600 HiLoadpg, GE Healthcare) equilibrated with Buffer A. All purification steps were carried out at 4°C using ÄKTA-Prime Plus FPLC system (GE healthcare). The fractions containing the protein were analysed on a 12% SDS PAGE and were concentrated using Amicon Ultra centrifugal filters (Merck, Millipore), flash-frozen in liquid nitrogen and stored at –80°C for further use.

Protein crystallization, structure determination and refinement

D2–Zn–WH$^{\Delta 2Y564A}$ was purified using Ni-NTA (HisTrap FF Crude Ni-NTA column) and size exclusion chromatography (S-200 HiLoad 16/600 pg column) as described previously. The protein was buffer exchanged using Amicon Ultra centrifugal filter (MWCO 10 kDa) in 10 mM Tris–HCl (pH 7.5), 50 mM NaCl and 2 mM DTT and used for crystallization on the same day without freezing. Initial crystallization hits were obtained by sitting drop vapour diffusion method at 25°C from the Index screen (Hampton Research, USA). The protein was concentrated to 12 mg ml^{-1} and was mixed 1:1 (v/v) with reservoir solution containing 60% (v/v) Tacsimate (1.8305 M malonic acid, 0.25 M ammonium citrate tribasic, 0.12 M succinic acid, 0.3 M DL-malic acid, 0.4 M sodium acetate trihydrate, 0.5 M sodium formate, and 0.16 M ammonium tartrate dibasic) at pH 7.0. Diffraction quality crystals were grown using hanging drop vapour diffusion method at 25°C, by mixing 1 μl of protein solution with 1 μl of reservoir solution containing 65% v/v Tacsimate pH 7.0. Plate like crystals appeared after 48 h of incubation. The crystals were cryoprotected with 10% (v/v) glycerol in mother solution and flash-cooled

in a nitrogen stream at 100 K. Diffraction data were collected on Rigaku Micromax HF007 Microfocus rotating-anode X-ray generator (Cu $K\alpha$ X rays, $\lambda = 1.5418$ Å) operated at 40 kV and 30 mA equipped with a Rigaku R-AXIS IV++ detector and a Varimax mirror system. A total of 180 frames of data were collected with an oscillation range of $1°$, an exposure time of 2 min per frame and a crystal-to-detector distance of 200 mm. Crystals diffracted to a maximum resolution of 2.8 Å. The data were processed with XDS (21). Space group was determined using POINTLESS (22), and scaling was done with SCALA (22). D2–Zn–WH$^{\Delta 2Y564A}$ crystallized in $P2_1$ space group, with two molecules per asymmetric unit. The structure was solved by molecular replacement using PHASER (23), with the structure of RECQ1^{T1} (PDB accession code: 2V1X) as the search model. Further refinement and chain fitting were done in PHENIX (24) and COOT (25). Data collection and refinement statistics are summarized in Table 1. The atomic coordinates and structure factors of D2–Zn–WH$^{\Delta 2Y564A}$ have been deposited in the Protein Data Bank with a PDB ID of 6JTZ.

Interface analysis

The interface between the Zn-binding domain (ZND) and WH domain was identified by comparing the solvent-accessible surface area (SASA) of the complex and the isolated domains. From the RECQ1 crystal structure (2V1X), we reconstructed the isolated chain A corresponding to D1–D2–Zn (residues 63–480) and chain B corresponding to WH domain (residues 481–592) and estimated the buried surface area (BSA) using Equation (1).

$$BSA = SASA(A) + SASA(B) - SASA(AB) \qquad (1)$$

where AB is the bound structure containing both the chains. We used Lee and Richard algorithm (26), implemented in the Naccess (27), to calculate the SASA. After identifying the interface residues from both the domains, we calculated the frequency of interactions within a cut-off distance of 4.5 Å to estimate the key binding residues at the interface.

Preparation of the DNA substrates

The oligonucleotides used for the strand annealing and DNA binding assays (11,15,16) were obtained from Integrated DNA Technologies, USA (listed in Supplementary Table S2). For radioactivity based assays, oligonucleotides (Rec20 and Fork30T_R) were labelled at the 5′ end with γ^{32}P-ATP using T4 polynucleotide kinase (NEB) at 37°C for 1 h. The unincorporated γ^{32}P-ATP was removed using nucleotide removal kit (QIAquick, QIAGEN, Germany). For DNA unwinding assays, fork duplex DNA was prepared by annealing 5′ end labelled Fork30T_R with 3-fold molar excess of an unlabelled complementary strand in a buffer containing 20 mM Tris–HCl, pH 7.5 and 50 mM NaCl. For the fluorescence anisotropy titrations, HPLC purified oligonucleotides labelled at 5′ end with 6-FAM (Rec20_FL or Fork30T_R_FL) were used. For the preparation of the double-stranded DNA substrates used in anisotropy titrations, unlabelled fully or partially

Table 1. Data collection, phasing and refinement statistics

Data collection and processing	
Wavelength(Å)	1.5418
Space group	$P2_1$
Cell dimensions (Å,°)	$a = 52.95$, $b = 101.83$, $c = 73.43$, $\beta = 99.07$
Resolution range (Å)	19.6–2.8 (2.9–2.8)
Total number of observations[a]	71 344 (10 221)
Number of unique reflections	18 892 (2709)
Multiplicity	3.8 (3.8)
Completeness (%)	99.0 (98.0)
R_{sym} (%)[b]	9
Rp.i.m.[c]	0.051 (0.218)
Average $I/\sigma(I)$	12.2 (3.9)
V_M (Å^3/Da)	2.44
$V_{solvent}$ (%)	49.51
Refinement statistics	
Resolution range (Å)	19.6–2.8
R_{work}/R_{free}[d]	0.227/0.280
Number of residues	
Protein	604
Solvent (waters)	139
Metal ion(Zn)	2
Ramachandran plot	
Favoured (%)	94.5
Allowed (%)	5
Outliers (%)	0.5
R.m.s.d., bonds (Å)	0.005
R.m.s.d., angles (°)	0.98
Average B factor (Å^2)	
Protein	39.08
Metal ion (Zn)	47.76
Solvent	33.09

[a]Numbers in parentheses refer to statistics for the outer resolution shell.
[b]$R_{sym} = 100 \cdot \Sigma_h \Sigma_i |I_i(h) - <I(h)>|/\Sigma_h \Sigma_i I_i(h)$, where $I_i(h)$ is the i-th measurement of reflection h and $<I(h)>$ is the average value of the reflection intensity.
[c]$R_{p.i.m.} = R_{merge} [1/(N-1)]^{1/2}$, where N is the data multiplicity.
[d]$R_{work} = \Sigma |F_{obs}| - |F_{cal}|/\Sigma |F_{obs}|$, where F_{obs} and F_{cal} are the structure factor amplitudes from the data and the model, respectively; R_{free} is same as R_{work} except that a 5% subset of all reflections was held aside throughout the refinement.

complementary oligonucleotides (Rec20R, Rec20R_3oh or Fork30T_F) were added to the 6-FAM labelled oligonucleotides in equimolar concentrations and heated to 95°C for 5 min and then cooled slowly to room temperature. Forked substrate used in ATP hydrolysis experiments was prepared using equimolar concentrations of unlabelled Fork30T_F and Fork30T_R and annealed using the same protocol as above.

Strand annealing assays

Strand annealing assays of all the RECQ1 constructs were carried out using fully or partially complementary oligonucleotides. The reaction was carried out at 25°C in the absence of ATP in a buffer containing 20 mM Tris–HCl pH 7.5, 10 mM NaCl, 1 mM β-ME, 10% glycerol and 80 μg/ml bovine serum albumin. ^{32}P-labelled single-stranded DNA (1.5 nM of Rec20 or Fork30T_R) was added to the reaction mix, followed by addition of the protein. Where specified, strand annealing reactions were carried out in the presence of different nucleotides such as ATP, ATPγS, ADP

and ADPNP at indicated concentrations. Reactions were started by addition of the complementary strand (2.5 nM of Rec20R or Fork30T_F). In reactions containing RPA70$^{\Delta C}$, both the labelled strand and the unlabelled complementary strand were pre-incubated with RPA70 $^{\Delta C}$ at indicated concentration for 5 min at 25°C in the reaction mixture. The reaction was initiated upon addition of RECQ1 constructs at specified concentrations ([17]). All the reactions were carried out at 25°C for 20 min and terminated using stop buffer (0.5% SDS and 10% Glycerol and 0.1% bromophenol blue). Reaction products containing 20 bp fully complementary blunt substrates were resolved on a 20% non-denaturing polyacrylamide gel. Reaction products containing the partially complementary fork substrates were resolved on a 12% non-denaturing polyacrylamide gel. The gel was run at 4°C and was visualised using phosphorimaging in Typhoon FLA 7000. Time course annealing assays were carried out for D2–Zn–WH, D2–Zn–WH$^{\Delta 2Y564A}$, D2–Zn–WH$^{\Delta helix}$ and D2–Zn–WH^{helix4A}. For all the constructs, the concentration of the protein used in each reaction was 100 nM. Reaction mixtures were incubated for different time points at 25°C and then terminated using stop buffer. Reaction products were resolved on a 20% non-denaturing polyacrylamide gel at 4°C and were visualised using phosphorimaging in Typhoon FLA 7000. The gels were analysed using image processing and analysis software Image J 1.46r and the percentage of DNA annealed was calculated for each lane ([28]). The percentage of spontaneous annealing in the enzyme-free control was calculated and subtracted from each lane. The data shown represent the mean of three independent experiments, with error bars indicating standard deviation. The concentration of enzyme required for 50% annealing was calculated from the plots.

DNA unwinding assays

DNA unwinding assays were carried out in the presence of 1 nM 5′-^{32}P labelled forked duplex DNA in a reaction buffer containing 20 mM Tris–HCl pH 7.5, 25 mM NaCl, 5 mM MgCl$_2$, 1 mM β-ME, 10% glycerol and 80 μg/mL bovine serum albumin. The enzyme was added at indicated concentrations, and the reactions were initiated by adding ATP at a specified concentration. The unwinding reaction was carried out at 37°C for 30 min and then terminated using stop buffer (0.5% SDS, 0.1M EDTA, 5% glycerol and 0.1% bromophenol blue). The products were resolved on a 12% non-denaturing PAGE run at 4°C and visualized using phosphorimaging in Typhoon FLA 7000.

Steady-state ATPase assay

ATP hydrolysis activity was studied using a coupled AT-Pase assay and measured as a decrease in A_{340} corresponding to oxidation of NADH to NAD$^+$ ([29]). The reaction was carried out in presence of saturating concentration of forked duplex DNA in a buffer containing 50 mM Tris–HCl pH 7.5, 10 mM MgCl$_2$, 0.1 mM β-ME, 0.4 mM phosphoenolpyruvate, 0.2 mM NADH, 23 mg.ml^{-1} lactate dehydrogenase, 37 mg.ml^{-1} pyruvate kinase, 20 mM NaCl and increasing ATP concentrations. The reaction was initiated by adding the enzyme at specified concentrations. The initial

velocities (in mM ATP s^{-1}), were calculated from the change in absorbance $\Delta A_{340}/t$ with $\varepsilon_{340, NADH} = 6220$ M^{-1}cm^{-1}, and were converted to k_{cat}. The values obtained were fitted to Michaelis-Menten equation, and K_M for ATP was determined. All experiments were repeated at least three times, and the data represent the mean of three independent experiments with error bars indicating the standard deviation.

Measurement of DNA binding using fluorescence anisotropy titrations

Binding of different DNA substrates to RECQ1 truncated constructs and full-length RECQ1 was studied by equilibrium fluorescence anisotropy titrations ([29,30]). Anisotropy titration experiments with D2–Zn–WH, D2–Zn–WH$^{\Delta 2Y564A}$, D2–Zn–WH^{helix4A} were carried out at 25°C in a reaction buffer containing 50 mM Tris–HCl (pH 7.5), 20 mM NaCl, 5 mM MgCl$_2$, and 0.1 mM β-ME. 10 nM of 5′ 6-FAM labelled substrates (a 20-mer single-stranded DNA, a 20 bp blunt ended duplex DNA, and a 20/10-mer duplex having a 3′ tail) were titrated using varying enzyme concentrations in a Fluoromax-4 fluorimeter (Horiba). Anisotropy titrations for RECQ1^{FL} were also performed in the presence of all the above-mentioned substrates under same reaction conditions.

Anisotropy titration experiments with RECQ1^{T1} and RECQ1^{T1,helix4A} were carried out in the same buffer in the presence of 5 mM ADPNP, and 10 nM of 5′ 6-FAM labelled fork duplex DNA substrate at 37°C. The excitation and emission wavelengths were fixed at 490 and 517 nm, respectively. All fluorescence anisotropy values were converted to fraction of DNA bound (f_B). For constructs D2–Zn–WH^{helix4A}, RECQ1^{T1}, RECQ1^{T1,helix4A} and RECQ1^{FL}, the data obtained were fitted to a quadratic function describing 1:1 binding (Equation [2]) using Origin 8.5 and dissociation constants (K_d) of the enzyme / DNA complex were determined.

$$f_B = \frac{1}{[DNA]_{tot}}$$
$$\left(\frac{[E]_{tot}+[DNA]_{tot}+K_d}{2} - \sqrt{\left\{ \left(\frac{[E]_{tot}+[DNA]_{tot}+K_d}{2} \right)^2 - [E]_{tot}[DNA]_{tot} \right\}} \right) \quad (2)$$

In the above equation, f_B is the fraction of DNA bound, which is calculated from the equation, $f_B = (r - r_0)/(r_{max} - r_0)$, where '$r$' is the observed anisotropy, r_0 is the initial anisotropy of the free dye, and r_{max} is the anisotropy at saturation. $[E]_{tot}$ is the total enzyme concentration, and $[DNA]_{tot}$ is the total DNA concentration. For constructs exhibiting cooperative binding (D2–Zn–WH and D2–Zn–WH$^{\Delta 2Y564A}$) data was fitted to Hill equation and the dissociation constants (K_d) of the enzyme/DNA complex were determined using Origin 8.5. All experiments were performed at least three times, and the data shown represent the mean of three independent experiments, with error bars indicating standard deviation.

Limited proteolytic digestion

Limited proteolysis experiments were carried out as described earlier ([11,17]). 5 μg of purified RECQ1^{T1} or RECQ1^{T1,helix4A} was incubated with chymotrypsin (0.05 μg) at 25°C for 1 h in presence of 5 mM MgCl$_2$ and in

the presence or absence of ATP or ATPγS (5 mM). The reaction was terminated by the addition of 5× SDS sample buffer and boiling for 5 min. The digested products were resolved on a 12% denaturing polyacrylamide gel and visualised by staining with Coomassie Blue.

RESULTS

Mutations on the β-hairpin restore strand annealing activity of annealing deficient construct D2–Zn–WH

As reported previously, the mutant RECQ1[T1] retains the ability to unwind forked duplex, whereas it completely lacks the strand annealing activity. Mutation at the tip of the β-hairpin in RECQ1[T1] leads to the restoration of the annealing activity [15,16]. These earlier findings can easily argue for the hypothesis that lack of unwinding might have led to gain of annealing, and the two functions are mutually exclusive. Moreover, it was also reported that the isolated WH domain can efficiently perform strand annealing similar to the wild type enzyme while a larger fragment encompassing the D2–Zn–WH (amino acid 282–616) completely lacks annealing activity. We, therefore, created the deletion construct encompassing D2–Zn–WH domains of RECQ1, harbouring the Y564A mutation at the tip of β-hairpin and two residues deleted from either side of the tyrosine 564 (D2–Zn–WH[Δ2Y564A], shown in Figure 1A). In this construct, residues F561, T562, A565 and T566 were deleted, and Y564 was mutated to alanine, keeping A563 intact. The same mutations on RECQ1[T1] (RECQ1[T1Δ2Y564A]) were reported to restore strand annealing activity in the annealing deficient RECQ1[T1] [15,16]. The mutants were purified to homogeneity (Figure 1B) as described in materials and methods and both eluted as monomers. We tested the strand annealing activity of the mutants (Figure 1C-E) using a ^{32}P labeled 20-mer DNA substrate (1.5 nM) as described in materials and methods. The mutant D2–Zn–WH[Δ2Y564A] exhibits improved strand annealing activity compared to the fragment encompassing D2–Zn–WH (Figure 1C and D). While D2–Zn–WH exhibits negligible strand annealing activity (11%) at 200 nM, the β-hairpin mutant D2–Zn–WH[Δ2Y564A] exhibits 50% strand annealing at 70 nM (Figure 1F). This indicates that, strand annealing is restored due to the β-hairpin mutation on D2–Zn–WH fragment. Since the isolated WH domain is reported to perform strand annealing similar to the full-length enzyme, we compared the annealing activity of D2–Zn–WH[Δ2Y564A] with that of the isolated WH domain. The isolated WH domain can indeed efficiently anneal complementary strands (Figure 1E), with 50% annealing being observed at 27 nM (Figure 1F). Although the β-hairpin mutant D2–Zn–WH[Δ2Y564A] was not as efficient as the isolated WH domain, its annealing activity clearly improved several folds compared to D2–Zn–WH. We also created a truncated RECQ1 fragment encompassing residues 282–649 (D2-Zn-CT) and its β-hairpin mutant (D2-Zn-CT[Δ2Y564A]). D2-Zn-CT exhibited no strand annealing while D2-Zn-CT[Δ2Y564A] exhibited strand annealing activity similar to D2–Zn–WH[Δ2Y564A] (Supplementary Figure S1). 50% annealing was observed at 50 nM concentration of D2-Zn-CT[Δ2Y564A]. These results clearly indicate that the mutations on the β-hairpin can restore strand

annealing activity of a shorter RECQ1 fragment (D2–Zn–WH) lacking both unwinding and annealing. It, therefore, nullifies the hypothesis that lack of unwinding results in a gain of annealing activity. In order to test whether mutations on β-hairpin directly affect strand annealing, we also tested the annealing activity of isolated WH domain and WH[Δ2Y564A]. The isolated WH and WH[Δ2Y564A] show similar strand annealing activity (Supplementary Figure S1), indicating that the β-hairpin is not directly involved in strand annealing. Our results clearly argue in favour of the hypothesis that these mutations must have induced some conformational change in RECQ-CTD that helps the WH domain to achieve a more favourable orientation for strand annealing.

Crystal structure of D2–Zn–WH[Δ2Y564A] reveals weakening of significant interactions between Zn and WH domain

In an attempt to understand the conformational changes that might have been induced due to the Δ2Y564A mutation, we crystallized the D2–Zn–WH fragment of human RECQ1 harbouring the mutation Δ2Y564A on the β-hairpin. The protein D2–Zn–WH[Δ2Y564A] was purified to 95% homogeneity as a monomer in solution and was crystallized as described in materials and methods. Data collection and refinement statistics are summarized in Table 1 (PDB ID. 6JTZ). The structure consists of 2 protein chains, 2 zinc ions and 139 water molecules, with a working R-factor of 22.7% and R_{free} value of 28%. Both D2–Zn–WH and the mutant D2–Zn–WH[Δ2Y564A] eluted as a monomer from S200 column. Although the protein crystallized as a dimer under crystallization conditions, we assume at low concentrations used in annealing assays, it exists as a monomer. The structure clearly exhibits the presence of RecA like domain 2 (D2), the Zinc binding domain and the WH domain with a shortened β-hairpin (Figure 2A). Superimposition of the mutant structure with that of RECQ1[T1] reveals that the domains align perfectly with that of RECQ1[T1] (backbone RMSD of 0.4 Å) except for the β-hairpin structure. The mutations not only lead to shortening of the β-hairpin, but also a clear distortion of the hairpin structure is observed (Figure 2B). The $2F_o - F_c$ electron density map for the mutated β-hairpin is shown in Figure 2B (inset).

A careful investigation into the interface of Zn binding and WH domains indicate that several significant interactions are disrupted due to the mutations. In RECQ1[T1] structure (2V1X), I567 and S568 on the β-hairpin can potentially interact with F424 and S428 on an α-helix located in the Zn binding domain (Figure 2C) as evident from the interatomic distances (well below 4Å). In the crystal structure of the mutant protein D2–Zn–WH[Δ2Y564A], F424 and S428 moved apart from I567 and S568, thereby weakening or disrupting these interactions (Figure 2D).The side-chain hydroxyl of S428 in the mutant structure assumes a rotamer conformation different from that in the RECQ1[T1] structure (the $2Fo-Fc$ electron density map is shown in Supplementary Figure S2). As a result, its interactions with I567 and S568 are weakened, as evident from the increased interatomic distances (Figure 2D).Weakening of these interactions might have contributed to the destabilization of the
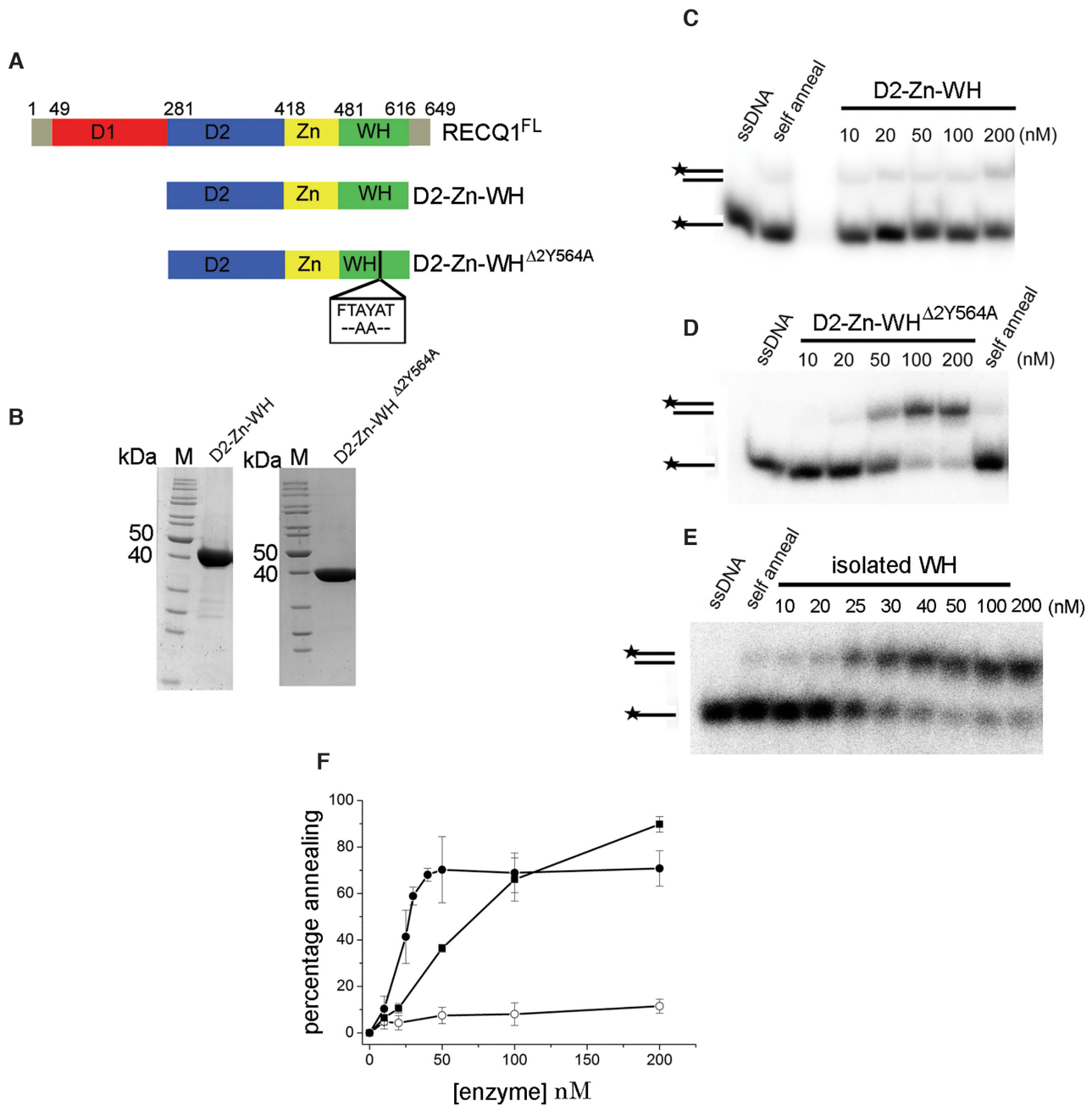
Figure 1. Analysis of strand annealing activity of RECQ1 truncated constructs and mutants. (**A**) Schematic representation of the domains of human RECQ1 and truncated constructs. The domain boundaries are marked with corresponding amino acid residue numbers. The β-hairpin mutation in the construct D2–Zn–WH$^{\Delta 2Y564A}$ is shown in the box. (**B**) SDS-PAGE analysis of purified RECQ1 constructs. The purified D2–Zn–WH and D2–Zn–WH$^{\Delta 2Y564A}$ were analysed by 12% SDS-PAGE. The molecular mass standard (M) is indicated on the left. (**C**) Strand annealing assay using increasing concentrations (10–200 nM) of D2–Zn–WH. (**D**) Strand annealing assay using increasing concentrations (10–200 nM) of D2–Zn–WH$^{\Delta 2Y564A}$ (**E**) Strand annealing assay using increasing concentrations (10–200 nM) of isolated WH. All annealing assays in C, D and E were performed using 1.5 nM of ^{32}P-labelled 20-mer sense strand and 2.5 nM of unlabelled 20-mer anti-sense strands. Lanes indicating 'ssDNA' contain 1.5 nM of ^{32}P-labelled sense strand only. Lanes indicating 'self-anneal' contain spontaneous annealing in the absence of enzyme. Reactions were carried out at 25°C for 20 min and products were resolved on 20% non-denaturing PAGE, and visualised using phosphorimaging in Typhoon FLA 7000. (**F**) Plot showing a comparison of the percentage of annealing by D2–Zn–WH (○), D2–Zn–WH$^{\Delta 2Y564A}$ (■) and isolated WH (●). The percentage of DNA annealed was plotted against protein concentration. Data represent the mean of three independent experiments, with standard deviation shown as error bars.
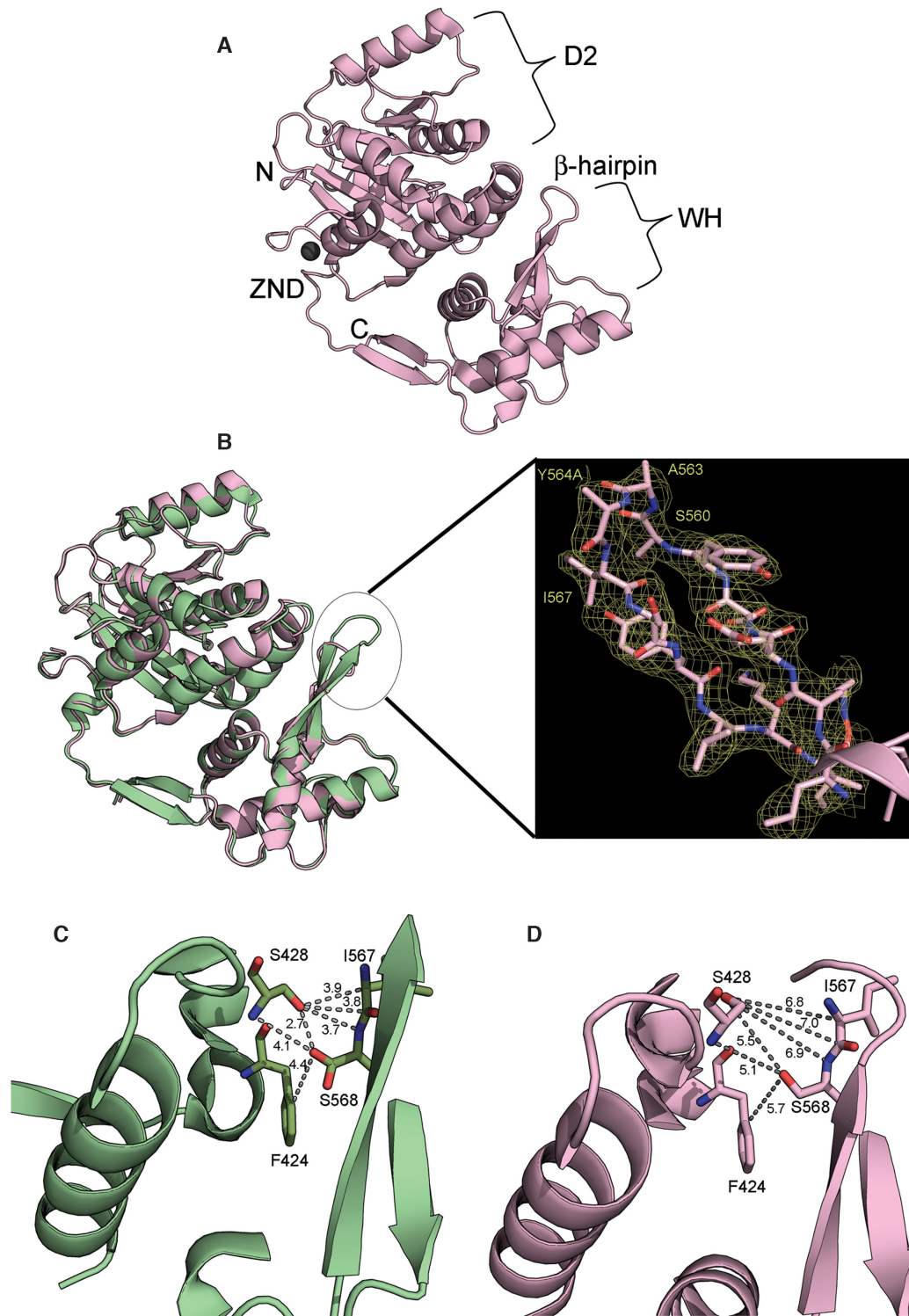
Figure 2. Overview of the structure of human RECQ1 truncated mutant D2–Zn–WH $^{\Delta 2Y564A}$. (**A**) Cartoon representation of a single monomer of D2–Zn–WH$^{\Delta 2Y564A}$ (light pink). Different subdomains are indicated: Core Helicase Domain2 (D2), Zn Binding Domain (ZND) and the Winged Helix Domain (WH) containing the mutated shortened β-hairpin motif. Zn metal ion in the zinc-binding domain is shown in sphere (grey) representation (generated in PyMOL v1.7) (PDB accession code: 6JTZ). (**B**) Structural superimposition of D2–Zn–WH$^{\Delta 2Y564A}$ (light pink) and RECQ1^{T1} (pale green). The structure of RECQ1^{T1} was taken from Pike *et al.* 2009 (PDB ID code: 2V1X). The shortened β-hairpin in the D2–Zn–WH$^{\Delta 2Y564A}$ structure does not align with the β-hairpin of RECQ1^{T1}. The sigma-A weighted $2F_o - F_c$ electron density map is shown for the mutated β-hairpin. The map is contoured at 1σ. (**C**) A closer view of the ZND–WH interface in RECQ1^{T1} showing the major interatomic distances between residues on β-hairpin and the α-helix on the ZND. All interatomic distances shown are well below 4.5Å. The side chain of S568 is shown with hydroxyl groups modelled in two different rotamers (occupancy = 0.5). (**D**) A closer view of the ZND-WH interface in D2–Zn–WH$^{\Delta 2Y564A}$, showing increased interatomic distances between residues on β-hairpin on WH domain and the α-helix on the ZND. All interatomic distances are measured in Å.

interface, thereby allowing the WH domain to orient in an annealing competent conformation. From the crystal structure, it is also evident that other significant interactions like S427:S568 and V431:Y559 are weakened in the β-hairpin mutant, thereby further contributing to the destabilization of the interface. It is, therefore, logical to hypothesize that weakening of interactions between the Zn binding residues and WH domain might have resulted in a conformational change favourable for efficient strand annealing by D2–Zn–WH[Δ2Y564A].

Analysis of the interface between Zn and WH domains reveals significant interactions of WH domain with an α-helix on Zn domain

The crystal structure of D2–Zn–WH[Δ2Y564A] clearly indicated a weakening of interactions at the interface between Zn and WH domains which might have a contributory role in the restoration of strand annealing. We, therefore, speculate that interaction between Zn and WH domain residues stabilizes the inter-domain interface and attenuates strand annealing by restricting the WH domain in a closed conformation. Mutations on β-hairpin destabilize the interface by weakening the interactions and, in turn, allow the WH domain to assume an open conformation more favourable for strand annealing. To gain further insight into the domain-domain interactions, we analyzed their interface by calculating buried surface area (BSA) as indicated in materials and methods. From the crystal structure of RECQ1[T1] (2VIX), we reconstructed the isolated chains corresponding to D1–D2–Zn (63–480) and the WH (481–592) domains. We calculated the solvent-accessible surface area (SASA) of the isolated chains (D1–D2–Zn and WH separately), as well as the complete structure containing all domains using Naccess tool (27), which implements Lee and Richard algorithm (26). Our results indicate that the solvent-accessible surface area (SASA) for the entire complex (63–592) is 23987.9 Å^2, while that of the isolated chains are 18831 Å^2 (D1–D2–Zn) and 6994.3 Å^2 (WH). The calculated BSA between the two domains is 1837.5 Å^2. This is more than 1.5 times higher than the average monomeric domain-domain interfaces (31,32), indicating a well defined and stable interface between the two domains (Figure 3A). Upon identifying the interface, we selected the key interacting residues by setting a cut-off distance of 4.5 Å. A summary of potential key interacting residues is listed in Table 2. Our results indicate that F420, F424, S427 and S428 have maximum number of interactions with the residues in the WH domain. F420 is likely to make significant contacts with E543, I546 and A547 (Figure 3B), while F424 has extensive contacts with E557, S568 and L570 (Figure 3B). The residues S427 and S428 make significant contacts with Y559 and S568 on the β-hairpin (Figure 3B). All these four residues are located on an α-helix (420–430) in the Zn domain facing the WH domain. Interestingly, our crystal structure data also demonstrate that three of these interacting residues (F424, S427 and S428) moved away from the WH domain residues (I567 and S568) in case of the D2–Zn–WH[Δ2Y564A] mutant, thereby weakening the interactions. Therefore, findings from our interface analysis are in line with the crystal structure data and strongly establish

the significance of these interactions in stabilizing the interface.

Deletion of the α-helix in Zn-domain restores strand annealing activity of annealing deficient construct D2–Zn–WH

From our crystal structure data, we hypothesized that destabilization of the interface due to Δ2Y564A mutation in D2–Zn–WH might have resulted in a conformation of the WH domain more favourable for performing strand annealing. Further analysis of the interface region between the Zn-binding and WH domains revealed potential interactions that might have a significant role in stabilizing the interface. We identified 4 major residues (F420, F424, S427 and S428) located on the α-helix in Zn-domain that can potentially interact with residues in the WH domain (listed in Table 2) and help in stabilizing the interface. To establish our hypothesis, we constructed a mutant of D2–Zn–WH lacking the entire α-helix encompassing residues 420–430 in the Zn domain (D2–Zn–WH[Δhelix]). We also created a mutant of D2–Zn–WH protein harbouring four mutations on the α-helix (F420A, F424A, S427A and S428A). The latter mutant harbouring the four mutations is named D2–Zn–WH[helix4A]. In both the mutants D2–Zn–WH[Δhelix] and D2–Zn–WH[helix4A], the β-hairpin was kept intact (Figure 4A). The proteins were purified to homogeneity (Figure 4B) as described in materials and methods and both proteins eluted as monomers. We tested the ability of both mutants in strand annealing assay as described (Figure 4C and D). Interestingly both the mutants were found to be efficient in strand annealing. 50% strand annealing was observed at 12 nM concentration of D2–Zn–WH[Δhelix], and almost 75% substrate was annealed at 30 nM enzyme concentration (Figure 4C and E). The mutant D2–Zn–WH[helix4A] also exhibits efficient strand annealing activity starting from 10 nM, and 50% annealing was observed at 25 nM enzyme concentration (Figure 4D and 4E). Interestingly, compared to the isolated WH domain, both the mutants (D2–Zn–WH[Δhelix] and D2–Zn–WH[helix4A]) exhibit more efficient strand annealing activity. While D2–Zn–WH[helix4A] has annealing activity similar to the WH domain, the mutant D2–Zn–WH[Δhelix] exhibits 50% annealing only at 12 nM concentration. These results clearly depict that deletion of or mutations on the α-helix not only restores strand annealing activity of D2–Zn–WH but also results in more efficient strand annealing by the mutants.

RECQ1 is known to physically and functionally interact with human replication protein A (RPA), leading to stimulation of unwinding and inhibition of annealing activities (17). In order to assess whether the increased level of strand annealing observed for the mutants (D2–Zn–WH[Δhelix] and D2–Zn–WH[helix4A]) was actually due to increased enzyme activity, we tested the inhibitory effect of human RPA. In assays with RPA, we used a soluble deletion construct of RPA70 lacking 175 amino acids from the C-terminus (RPA70[ΔC]). It was shown that RPA70 lacking 175 amino acids from the C-terminus is soluble and is sufficient to stimulate the unwinding activity of WRN helicase (33,34). Moreover, it has also been reported that the DNA binding activity of RPA70 resides on the first 441 amino acids, and hence the construct RPA70[ΔC] is sufficient to in-
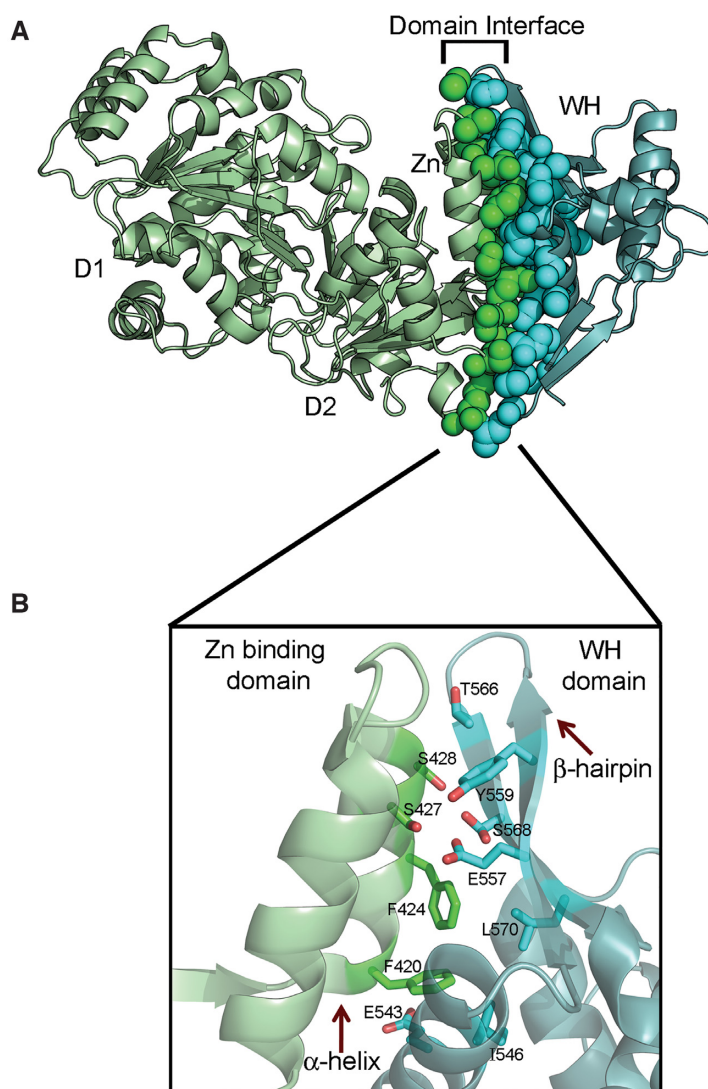
Figure 3. Analysis of the interface between Zn-binding domain and WH domain of RECQ1. (**A**) The interface between the Zn-binding domain and WH domain was analysed from the RECQ1 crystal structure (2V1X, Pike *et al.*, 2009) by calculating the buried surface area (BSA) using Naccess tool (27). The residues contributing to the interface are indicated by spheres (Green spheres for Zn-domain residues and cyan spheres for WH residues). For better visualisation, the D1, D2 and Zn-domain are represented in pale green colour, while WH is represented in teal (blue-green) colour. (**B**) A closer view of the identified interface residues between the Zn binding domain and WH domain falling within a cut-off distance of 4.5 Å. Interface residues constituting F420, F424, S427, S428 in the α-helix of Zn-binding residues (residues 420–430) and E543, I546, E557, Y559, T566, S568, L570 in the β-hairpin of the winged-helix domain (residues 554–573) are shown in stick representation (Figure generated in PyMOL V1.7. The side chain of S568 is shown with hydroxyl groups modelled in two different rotamers (occupancy = 0.5).

hibit strand annealing activity (33). Strand annealing was indeed inhibited by the addition of RPA70$^{\Delta C}$ in annealing reactions, and complete inhibition was achieved at 100 nM of RPA70$^{\Delta C}$ in case of both the mutants (Figure 4F and G). In an attempt to understand the contribution of these mutations in strand annealing kinetics, we performed time-course annealing experiments with D2–Zn–WH, D2–Zn–WH$^{\Delta2Y564A}$, D2–Zn–WH$^{\Delta helix}$and D2–Zn–WH^{helix4A} (Figure 5A–D). D2–Zn–WH is inefficient in strand annealing and can only anneal up to 20% of the substrate even after 60 min of reaction, while D2–Zn–WH$^{\Delta2Y564A}$ can anneal 60% within the first 15 min of reaction. The mutants D2–Zn–WH$^{\Delta helix}$ and D2–Zn–WH^{helix4A} are highly efficient in strand annealing, and both the mutants can anneal 90% of

the substrate within the first 10 min of reaction (Figure 5E). These results clearly indicate that mutations on the α-helix render the enzyme more efficient in strand annealing that might be attributed to the destabilization of the interface. The results strongly argue in favour of our hypothesis that disruption of the interface by introducing mutations on the α-helix or deletion of the α-helix allows the WH domain to orient in a preferred conformation that favours strand annealing.

Mutations on the α-helix in Zn-domain affect DNA binding

In order to understand the correlation between DNA binding and strand annealing activity of the mutants, we

Table 2. List of major interface residues

Residues on the Zn-binding domain	Residues on the winged helix domain
Phe 420	Glu 543
	Ile 546
	Ala 547
Phe 424	Ser 568
	Glu 557
	Leu 570
Ser 427	Tyr 559
	Glu 557
	Ser 568
Ser 428	Tyr 559
	Ser 568
	Thr 566
	Ile 567
Val 431	Tyr 559
	Phe 561
	Thr 566
Tyr 441	Ile 551
	Glu 557
	Gln 553
	Leu 550
Gln 448	Lys 554
	Ile 551
	Ala 547
	His 548
	Met 588
Ile 450	Phe 484
	Gln 589
	Lys 544
	Val 490
	Thr 591

assessed DNA binding affinities of the annealing deficient and annealing competent mutants of RECQ1 using fluorescence anisotropy (Figure 6). 5′-6-FAM labelled ssDNA, dsDNA (blunt duplex) and 3′ tailed duplex substrates were used in the assay. The sequences of the oligonucleotides used are listed in Supplementary Table S2. The results of fluorescence titrations are summarized in Table 3. There was no significant difference observed in ssDNA affinity of D2–Zn–WH and D2–Zn–WH$^{\Delta 2Y564A}$, as evident from the dissociation constants (Table 3, Figure 6A). This was expected; since mutations on β-hairpin is not likely to affect ssDNA binding. A 1.5-fold decrease in dsDNA binding ($K_d = 1.78$ μM) and 3′-tailed duplex binding ($K_d = 2.75$ μM) was observed (Figure 6B and C, Table 3) for D2–Zn–WH$^{\Delta 2Y564A}$ as compared to D2–Zn–WH (1.17 μM and 1.97 μM respectively). Since the β-hairpin is known to be a major structural element in DNA recognition and unwinding, a 1.5-fold decrease in substrate binding due to mutations at the β-hairpin tip seems reasonable. On the other hand, we observed a significant loss in DNA binding for the α-helix mutant (D2–Zn–WH^{helix4A}) as compared to D2–Zn–WH or D2–Zn–WH$^{\Delta 2Y564A}$. There was almost 1.8-fold (2.08 ± 0.15 μM compared to 1.17 ± 0.12 μM for D2–Zn–WH) loss in dsDNA binding and 3-fold loss (5.7 ± 1.1 μM compared to 1.97 ± 0.3) in 3′ tailed duplex binding in case of D2–Zn–WH^{helix4A} as compared to D2–Zn–WH (Figure 6D and E). Single-stranded DNA (ssDNA) binding for the α-helix mutant could not be determined in the concentration range used for the anisotropy titrations. This significant loss in DNA binding and its correlation to DNA strand anneal-

ing needs careful interpretation and further investigations. It is possible that mutation of residues on the α-helix induces a severe conformational change in the WH domain, thereby restricting it to a conformation not favourable for substrate binding but favourable for strand annealing. Interestingly, D2–Zn–WH and D2–Zn–WH$^{\Delta 2Y564A}$ exhibit co-operativity in DNA binding (Figure 6A and B) for ssDNA and blunt dsDNA substrates while the mutant D2–Zn–WH^{helix4A} exhibits 1:1 binding. It is possible that the mutants D2–Zn–WH and D2–Zn–WH$^{\Delta 2Y564A}$ oligomerize in the presence of ssDNA and blunt duplex and hence exhibit co-operative binding. The mutant D2–Zn–WH^{helix4A} undergoes severe conformational change due to destabilization of the interface between Zn and WH domain and attains a conformation that is unfavourable for DNA binding and oligomerization.

We also assessed the DNA binding affinities of the full-length RECQ1 (RECQ1^{FL}) with all the DNA substrates used in the study (Supplementary Figure S3) and compared with that of the D2–Zn–WH fragments. As expected, the full-length RECQ1 can bind all the DNA substrates (ssDNA, blunt duplex and 3′ tail DNA) with much higher affinities (see Table 3) compared to the shorter fragments. The differences in DNA binding observed for the mutants D2–Zn–WH$^{\Delta 2Y564A}$ and D2–Zn–WH^{helix4A} with respect to D2–Zn–WH remain significant when compared to that of full-length RECQ1. While D2–Zn–WH exhibits 8.5-fold lesser affinity for 3′ tailed DNA with respect to RECQ1^{FL} (1.97 μM compared to 0.23 μM for RECQ1^{FL}), the mutant D2–Zn–WH^{helix4A} exhibits 25-fold loss in binding compared to RECQ1^{FL} (5.17 μM compared to 0.23 μM for RECQ1^{FL}). Similarly, for the blunt dsDNA substrate, D2–Zn–WH fragment exhibits a 4-fold lesser binding (1.17 μM compared to 0.28 μM) while a 7.5-fold loss in binding was observed for the mutant D2–Zn–WH^{helix4A} (2.08 μM compared to 0.28 μM) as compared to full-length RECQ1. These results further confirm that the observed differences in DNA binding among the RECQ1 shorter fragments are highly significant and may be attributed to conformational changes within the Zn and WH domains. Moreover, the full-length enzyme exhibits DNA stimulated ATPase activity (Supplementary Figure S3B) while the shorter fragments completely lack the ATPase activity in presence of DNA. This indicates that the conformational change in the shorter fragments is independent of ATP binding and is more likely due to the destabilization of the interface resulting in a weaker DNA binding. The DNA binding results and their possible implications in strand annealing have been discussed more in the discussion section. Results from our DNA binding experiments indicate that mutations on the α-helix (420–430) affect substrate binding significantly even if the β-hairpin remains intact. The observed results strongly argue in favour of the hypothesis that a major conformational change in the RQC domain is responsible for the reduced DNA binding.

Mutations on the α-helix in Zn-domain restores strand annealing activity of annealing deficient RECQ1^{T1}

Our experimental evidence so far strongly argue in favour of the hypothesis that interaction of residues in the WH
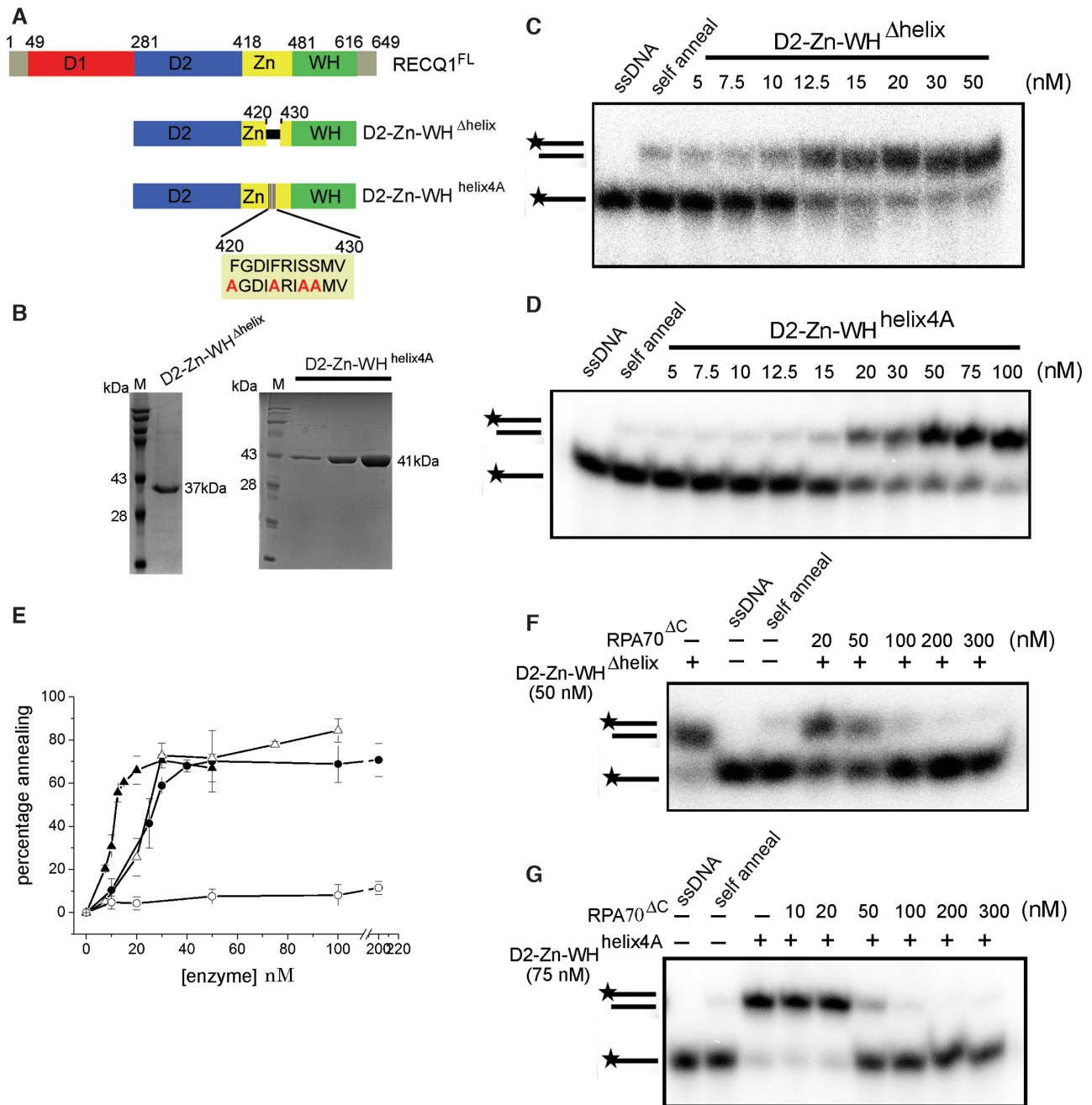
Figure 4. Analysis of strand annealing activity of truncated RECQ1 constructs harbouring mutations in the zinc binding domain. (**A**) Schematic representation of the domains of human RECQ1 and truncated constructs. The domain boundaries are marked with corresponding amino acid residue numbers. The deletion of the α-helix in the construct D2–Zn–WH$^{\Delta helix}$ in the Zn- binding domain is represented by a small gap within the domain. The mutation of four amino acids in the Zn- binding domain is shown in the box. The upper line in the box shows the original (wild type) sequence, while the lower line shows the sequence of the α-helix containing the mutations. (**B**) SDS- PAGE analysis of purified RECQ1 constructs. The S-200 purified D2–Zn–WH$^{\Delta helix}$ and D2–Zn–WH^{helix4A} were analysed by 12% SDS-PAGE. The molecular mass standard (M) is denoted on the left. (**C**) Strand annealing assay using increasing concentrations of D2–Zn–WH$^{\Delta helix}$ (5–50 nM). (**D**) Strand annealing assay using increasing concentrations of D2–Zn–WH^{helix4A} (5–100 nM). Annealing assays were performed using 1.5 nM of ^{32}P-labelled 20-mer sense strand and 2.5 nM of unlabelled anti-sense strands containing increasing enzyme concentrations as indicated on the lanes. Lanes indicating 'ssDNA' contain 1.5 nM of ^{32}P-labelled sense strand. Lanes indicating 'self-anneal' indicates spontaneous annealing in the absence of enzyme. All reactions were carried out at 25°C for 20 min, and products were resolved on 20% non-denaturing PAGE and visualised using phosphorimaging in Typhoon FLA 7000. (**E**) Plot showing the percentage of annealing by D2–Zn–WH$^{\Delta helix}$ (▲) and D2–Zn–WH^{helix4A} (△) as compared to that of isolated WH (●) and D2–Zn–WH (○). The percentage of DNA annealed has been plotted against increasing protein concentration. Data represent the mean of three independent experiments, with error bars indicating standard deviation. **F.** Inhibition of strand annealing activity of D2–Zn–WH$^{\Delta helix}$ in the presence of increasing concentrations of RPA70$^{\Delta C}$ (20–300 nM). (**G**) Inhibition of strand annealing activity of D2–Zn–WH^{helix4A} in the presence of increasing concentrations of RPA70$^{\Delta C}$ (10–300 nM). Both the labelled and unlabelled complementary oligonucleotides were incubated with increasing concentrations of RPA70$^{\Delta C}$ at 25°C for 5 min. Annealing reactions were initiated by the addition of D2–Zn–WH$^{\Delta helix}$ (50 nM) or D2–Zn–WH^{helix4A} (75 nM) and was carried out at 25°C for 20 min. The products were resolved on 20% non-denaturing PAGE and visualised by phosphorimaging in Typhoon FLA 7000.
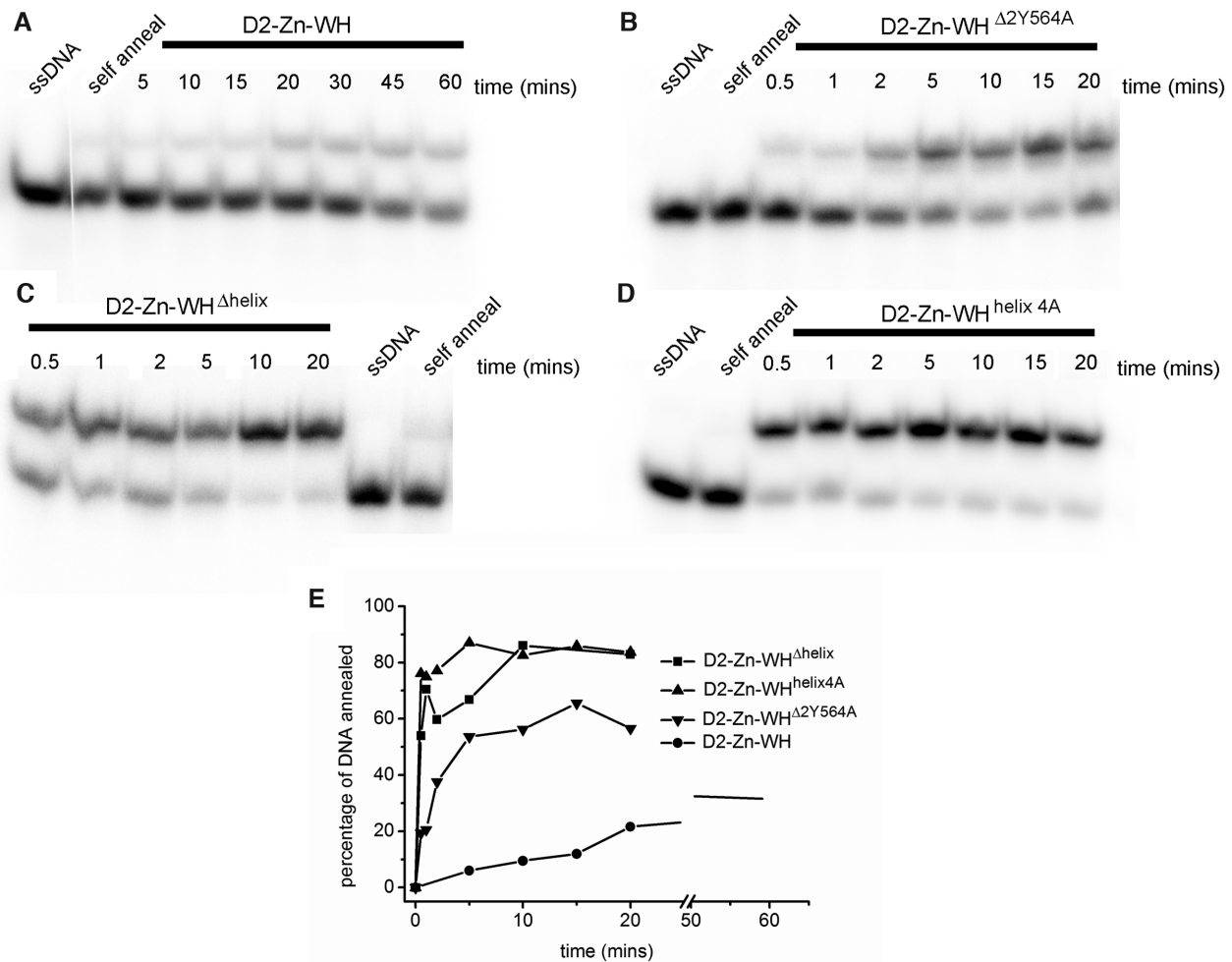
Figure 5. Time kinetics of the strand annealing activity to form a 20mer blunt duplex by different RECQ1 constructs. (**A**) D2–Zn–WH, (**B**) D2–Zn–WH$^{\Delta 2Y564A}$, (**C**) D2–Zn–WH$^{\Delta helix}$ and (**D**) D2–Zn–WH^{helix4A}. Time course annealing assays were performed using 1.5 nM ^{32}P-labelled sense strand and 2.5 nM of unlabelled anti-sense strand in the presence of 100 nM of truncated RECQ1 constructs. Lanes indicating 'ssDNA' contains only 1.5 nM of ^{32}P-labelled sense strand. Lanes indicating 'self-anneal' contains both sense and antisense strands but without enzyme. The reaction was initiated by the addition of anti-sense strand and terminated using a stop buffer at time points indicated on the respective lanes. (**E**) Quantitative analysis of the kinetics of formation of blunt duplex mediated by RECQ1 constructs. The percentage of strand annealing was plotted against respective time points.

domain with the α-helix in the Zn domain attenuates strand annealing activity of D2–Zn–WH fragment of human RECQ1. Our data also depicts that disruption of these interactions and subsequent destabilization of the domain-domain interface restores strand annealing and compromises DNA binding in these constructs. We, therefore, tried to extrapolate the same findings on the near full-length RECQ1 fragment RECQ1^{T1}. We created a mutant of RECQ1 lacking 48 amino acids in the N-terminus and 33 amino acids in the C-terminal region (RECQ1^{T1}, demonstrated in ref [11]) and harboring 4 mutations (F420A, F424A, S427A, S428A) on the α-helix in the Zn domain (RECQ1^{T1,helix4A}) (Figure 7A). The mutant RECQ1^{T1,helix4A} was purified as described (Figure 7B), and it eluted as a monomer (data not shown) in contrast to RECQ1^{T1}, which elutes as a dimer. We assessed the strand annealing activity of the mutant RECQ1^{T1,helix4A} and compared its activity with respect to RECQ1^{T1} using 20 mer DNA as well as fork DNA substrates (Figure 7C–F). While

RECQ1^{T1} can anneal only 10% of the substrate at 200 nM concentration (Figure 7C), the mutant RECQ1^{T1,helix4A} can efficiently anneal the 20 mer DNA substrate starting from 40 nM concentration (Figure 7D). In annealing reactions containing forked substrate, 50% annealing was observed at 6.5 nM RECQ1^{T1,helix4A} (Figure 7F and G) and almost 80% annealing was observed at 10 nM concentration of RECQ1^{T1,helix4A} while no annealing was observed in RECQ1^{T1} even at 200 nM (Figure 7E and G). The enzyme RECQ1^{T1,helix4A} turned out to be more efficient in strand annealing compared to the isolated WH domain and other annealing competent constructs lacking the D1 domain discussed earlier. These data suggest that disruption of the interface between Zn and WH domains can restore strand annealing activity of annealing deficient RECQ1^{T1} and hence confirms that our hypothesis can be extrapolated for the near full-length RECQ1 mutant. We also assessed the effect of RPA70$^{\Delta C}$ on strand annealing activity of RECQ1$^{T1, helix4A}$. RPA70$^{\Delta C}$ inhibited strand annealing ac-
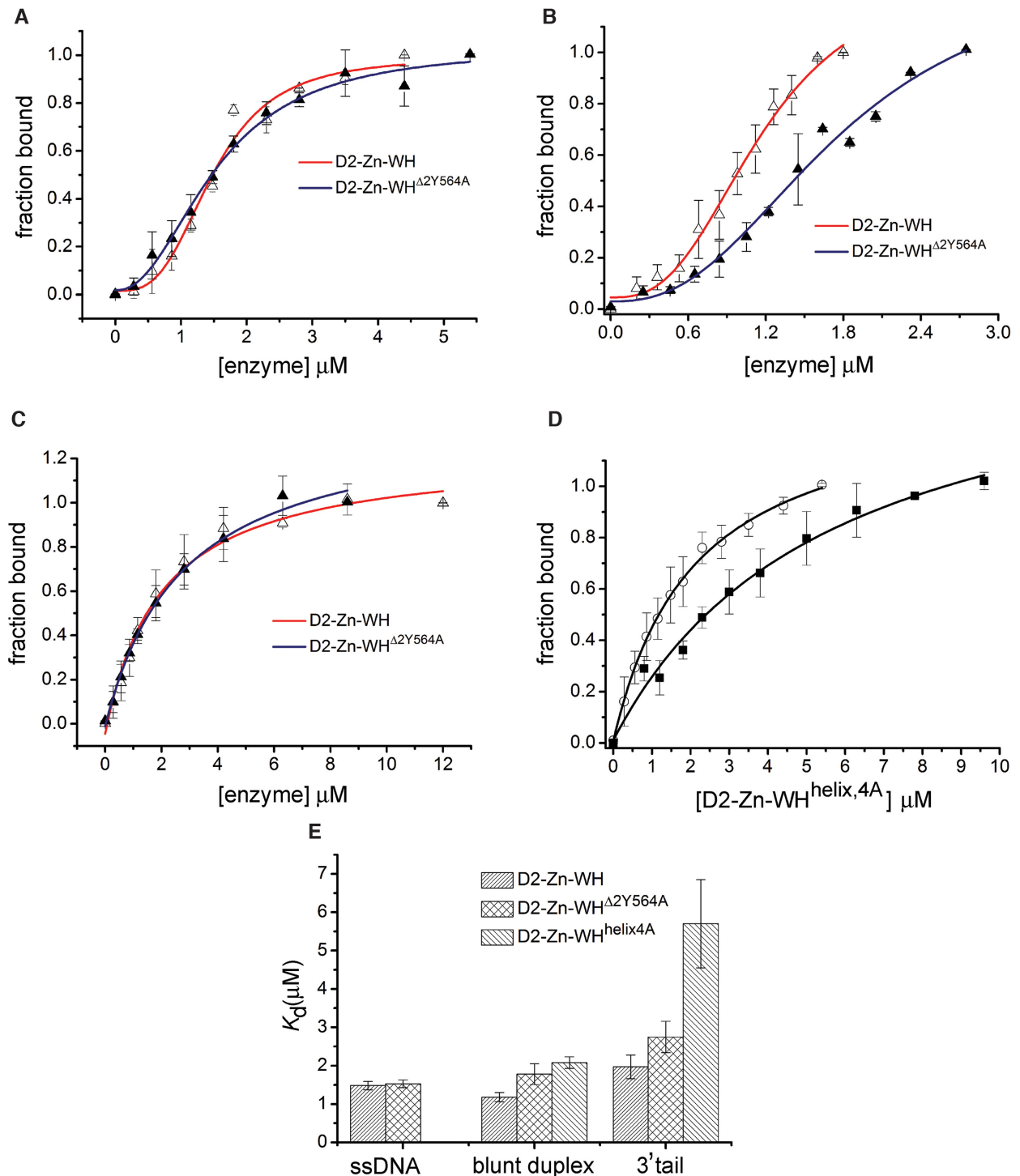
Figure 6. Measurement of DNA binding using fluorescence anisotropy titrations for D2–Zn–WH, D2–Zn–WH$^{\Delta 2Y564A}$ and D2–Zn–WH^{helix4A}. (**A**) Anisotropy titrations were performed in the presence of 10 nM, 5′ 6-FAM labelled single stranded DNA with D2–Zn–WH (red, $\triangle$) and D2–Zn–WH$^{\Delta 2Y564A}$ (blue, ▲). (**B**) Anisotropy titrations performed in the presence of 10 nM 5′ 6-FAM labelled blunt duplex DNA with D2–Zn–WH (red, $\triangle$) and D2–Zn–WH$^{\Delta 2Y564A}$ (blue, ▲). For both A and B, the anisotropy values were converted to fraction of DNA bound as described in materials and methods, and data were fitted to Hill equation, and dissociation constants (K_d) were calculated. (**C**) Anisotropy titrations performed in the presence of 10 nM 5′ 6-FAM labelled 20/10 mer 3′ tailed duplex DNA with D2–Zn–WH (red, $\triangle$) and D2–Zn–WH$^{\Delta 2Y564A}$ (blue, ▲). (**D**) Anisotropy titrations with D2–Zn–WH^{helix4A} performed in the presence of 10 nM 5′ 6-FAM labelled 20/10 mer 3′ tailed duplex (■) and 20 base paired blunt duplex DNA ($\bigcirc$). For both C and D, the anisotropy values were converted to fraction of DNA bound and the data were fitted using Equation (2) as mentioned in Materials and Methods, and dissociation constants (K_d) were calculated. For all titrations, data shown here are the mean of at least three independent experiments, and the error bars represent the standard deviation. (**E**) Histogram showing the comparison of dissociation constants (K_d) for different DNA substrates as obtained from experimental sets (A–D). The K_d values indicated here are the mean values obtained from three independent experiments. Error bars indicate SEM. The K_d values are also listed in Table 3.

Table 3. Dissociation Constants measured from fluorescence anisotropy titrations

Constructs	K_d (μM)		
	ssDNA	Blunt-duplex DNA	3'tailed DNA
D2–Zn–WH	1.48 ± 0.11 $n = 3.1$	1.17 ± 0.12 $n = 2.7$	1.97 ± 0.3
D2–Zn–WH$^{\Delta 2Y564A}$	1.53 ± 0.1 $n = 2.2$	1.78 ± 0.27 $n = 2.5$	2.75 ± 0.4
D2–Zn–WH^{helix4A}	ND	2.08 ± 0.15	5.7 ± 1.1
RECQ1^{FL}	0.14 ± 0.03	0.28 ± 0.04	0.23 ± 0.05

tivity of RECQ1^{T1,helix4A} starting from 50 nM concentration similar to that observed for the shorter mutants encompassing D2–Zn–WH domains (Figure 7H). This result indicates that the increased annealing observed for the mutant is indeed due to the increased enzymatic activity.

The strand annealing activity of RECQ1 is known to be inhibited in the presence of ATP. The mutant RECQ1^{T1,helix4A} retains the D1 domain and hence is expected to bind and hydrolyse ATP. In order to assess the effect of nucleotides on strand annealing activity of RECQ1^{T1,helix4A}, we performed the annealing reaction in the presence of ATP, ADP, ADPNP and ATPγS (Figure 7I). Similar to wild type RECQ1, the presence of nucleotides (5 mM ATP or non-hydrolysable analogues) inhibited strand annealing activity, although complete inhibition was not achieved at 2 mM ATP or ADPNP. In contrast to earlier findings with RECQ1^{FL} (17), where 2 mM ATP or ATPγS was sufficient to inhibit annealing activity, very little inhibition was observed at 2 mM ATP, ADP or ADPNP in case of RECQ1^{T1,helix4A}. Strikingly, 2 mM ATPγS significantly inhibited strand annealing of RECQ1^{T1,helix4A} similar to wild type RECQ1^{FL}. It is possible that mutations on the α-helix leads to significant conformational change in the RQC domain rendering the enzyme less responsive to ATP induced conformational change, and therefore requires higher ATP concentration (5 mM) to achieve a conformation that disfavours strand annealing. To validate this hypothesis, we performed limited proteolysis experiments with RECQ1^{T1} and RECQ1^{T1,helix4A} in the presence or absence of ATP and non-hydrolysable ATP analogue ATPγS. Limited proteolysis of both the mutants was performed using chymotrypsin for 1 h as described in materials and methods. There was a clear difference in proteolysis patterns for RECQ1^{T1} and RECQ1^{T1,helix4A} both in the absence and presence of ATP and ATPγS (Supplementary Figure S4). In the case of RECQ1^{T1}, two proteolysis resistant bands were observed near 40kDa and one near 30 kDa. A similar pattern was also reported for RECQ1^{T1} by Pike *et al.* (11). In case of RECQ1^{T1,helix4A}, no prominent bands were observed near 40 kDa or 30 kDa in the absence or presence of nucleotides indicating that the latter assumes a different conformation altogether. The results strongly argue in favour of the hypothesis that, mutations in the α-helix led to destabilization of the interface and resulted in an altered conformation of the RQC.

We also validated our findings in the full-length RECQ1 by introducing the same mutations in the full-length en-

zyme. The full-length RECQ1 and the mutant harboring the four mutations in α-helix (RECQ1^{FLhelix4A}) were expressed and purified using baculovirus expression system as described in materials and methods. Annealing experiments were performed using forked substrate in the presence of RECQ1^{FL} and RECQ1^{FLhelix4A}. The mutant enzyme exhibits improved strand annealing activity compared to the wild type RECQ1^{FL} (Supplementary Figure S5). Fifty percent annealing was achieved at 50 nM RECQ1^{FL}, and the level of annealing remained the same even at higher concentration. Pike *et al.*, 2015 also reported a similar degree of strand annealing of fork substrate by RECQ1^{FL}, where 50% annealing was achieved at 50 nM concentration (15). On the other hand, the mutant RECQ1^{FLhelix4A}, exhibits 50% annealing starting from 10 nM concentration, and the degree of annealing remains constant even at higher concentrations similar to the wild type. These results further confirm that the effects of mutation observed in near full-length mutant RECQ1^{T1} are also reflected in the full-length RECQ1, although 100% annealing was not achieved in the latter case. This difference in the highest level of annealing for RECQ1^{T1,helix4A} and RECQ1^{FLhelix4A} may be attributed to their different oligomeric states. Moreover, unlike RECQ1^{T1}, the wild type RECQ1^{FL} is already an annealing competent enzyme, and hence improvement rather than restoration of annealing activity is sufficient to indicate a functional difference between the two enzymes. Our results strengthen the notion that interactions at the interface between Zn and WH domains attenuate strand annealing activity. Weakening of these interface interactions induces a conformational change that restores annealing activity of RECQ1^{T1} and improves strand annealing activity of RECQ1^{FL}.

Mutations on the α-helix in Zn domain affect DNA stimulated ATP hydrolysis and weakens the unwinding activity of RECQ1^{T1}

Results from the annealing experiments and partial proteolysis with RECQ1$^{T1, helix4A}$ clearly indicated that the mutations in the α-helix on Zn domain induces major conformational change in the RQC domain, which is responsible for increased strand annealing activity of the mutant. Moreover, reduced sensitivity towards ATP mediated inhibition of annealing activity also indicates that the enzyme might have become less responsive to ATP induced conformational change. We, therefore, tested the ability of RECQ1^{T1,helix4A} and RECQ1^{T1} (Figure 8A and B) to unwind a forked duplex substrate in the presence of 5 mM ATP. Interestingly, our data shows that RECQ1^{T1,helix4A} is unable to unwind the forked substrate up to 30 nM enzyme concentrations in the presence of 5 mM ATP (Figure 8B, left panel), while RECQ1^{T1} can completely unwind the substrate at 20 nM in the presence of same ATP concentration (Figure 8A). A very feeble unwinding in case of RECQ1^{T1helix4A} was detectable when compared to the no ATP control (Figure 8B, lane next to ssDNA control). This was surprising since both the mutants have their β-hairpins intact. We next tried to assess the DNA stimulated ATP hydrolysis activity of RECQ1^{T1,helix4A} in the presence of forked substrate and compared it with the ATPase
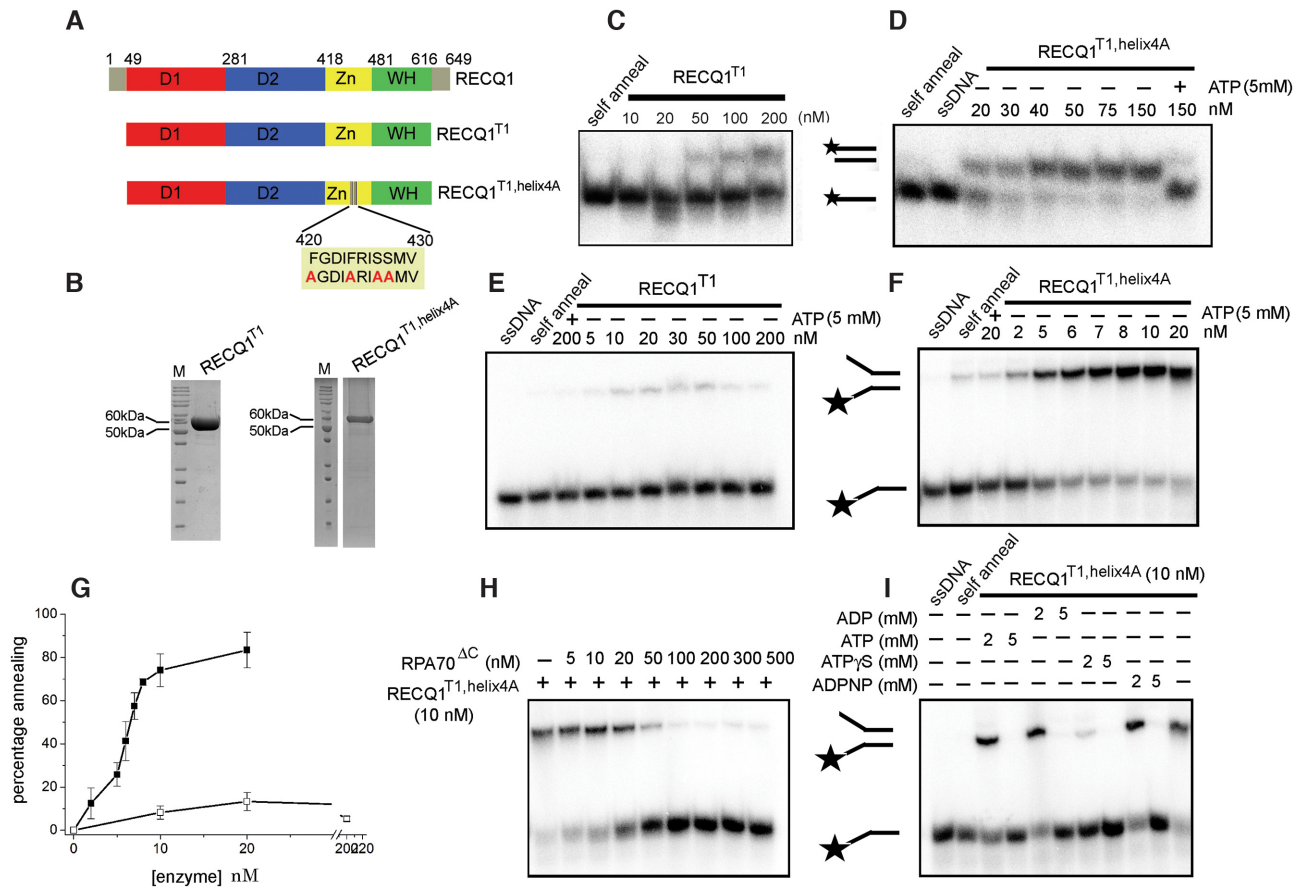
Figure 7. Analysis of strand annealing activity of RECQ1[T1] and its mutant RECQ1[T1,helix4A]. (**A**) Schematic representation of the domains of human RECQ1 and truncated constructs used. The domain boundaries are marked with corresponding amino acid residue numbers. The mutation of four amino acids in the Zn- binding domain is shown in the box. (**B**) SDS- PAGE analysis of purified RECQ1 constructs. The S-200 purified RECQ1[T1] and RECQ1[T1,helix4A] were analysed by 12% SDS-PAGE. The molecular mass standard (M) is denoted on the left. (**C**) Strand annealing assay in the presence of increasing concentrations of RECQ1[T1] (10–200 nM) using 20 mer fully complementary oligonucleotides. (**D**) Strand annealing assay in the presence of increasing concentrations of RECQ1[T1,helix4A] (20–150 nM). Annealing assay was performed using 1.5 nM of ^{32}P-labelled 20-mer sense strand and 2.5 nM of fully complementary unlabelled anti-sense strand. Reactions were carried out at 25°C for 20 min, and products were resolved on 20% non-denaturing PAGE, and visualised using phosphorimaging in Typhoon FLA 7000. (**E**) Strand annealing assay using increasing concentrations of RECQ1[T1] (5–200 nM) using partially complementary 50 mer oligonucleotides. (**F**) Strand annealing assay in the presence of increasing concentrations of RECQ1[T1,helix4A] (2–20 nM). Annealing assay was performed using 1.5 nM of ^{32}P-labelled 50-mer sense strand and 2.5 nM of partially complementary unlabelled anti-sense strands (forming a forked duplex upon annealing). Lanes indicating 'ssDNA' contain 1.5 nM of ^{32}P-labelled sense strand. Lanes indicating 'self-anneal' indicates spontaneous annealing in absence of enzyme. All reactions were carried out at 25°C for 20 min, and products were resolved on 12% non-denaturing PAGE and visualised using phosphorimaging in Typhoon FLA 7000. (**G**) Plot showing the strand annealing activity of RECQ1[T1] (□) and RECQ1[T1,helix4A] (■) as a function of the concentration of protein using partially complementary strands which form fork duplex substrate. The percentage of DNA annealed has been plotted against increasing protein concentration. Data represent the mean of three independent experiments, with error bars shown as standard deviation. (**H**) Inhibition of strand annealing activity of RECQ1[T1,helix4A] in the presence of increasing concentrations of RPA70[ΔC] (5–500 nM). Both the labelled and unlabelled partially complementary oligonucleotides were incubated with increasing concentrations of RPA70[ΔC] at 25°C for 5 min. The annealing reactions were initiated by addition of RECQ1[T1,helix4A] (10 nM) and was carried out at 25°C for 20 min. The products were resolved on 12% non-denaturing PAGE and visualised by phosphorimaging in Typhoon FLA 7000. (**I**) Effect of nucleotides and nucleotide analogues on strand annealing activity of RECQ1[T1,helix4A] (10 nM). Annealing of partially complementary oligonucleotides was assessed in the presence of 2 mM or 5 mM ATP, ADP, ATPγS and ADPNP at concentrations of 2 mM and 5 mM each. Concentrations of respective nucleotides are indicated on the lanes.

activity of RECQ1[T1] (Figure 8C). Interestingly, our data reveals that the α-helix mutant RECQ1[T1,helix4A] exhibits a much slower ATP hydrolysis rate in the presence of fork substrate with a k_{cat} of 5.2 min^{-1}, which is 16-fold lesser than that of RECQ1[T1] (84 min^{-1}). There was an ∼6-fold increase in $K_{M,ATP}$ in case of RECQ1[T1,helix4A] ($K_{M,ATP}$ = 0.22 mM) as compared to that of RECQ1[T1] ($K_{M,ATP}$ = 0.038 mM), indicating a decrease in affinity towards ATP. The ATP hydrolysis data strongly corroborates with the earlier findings and explains the weakening of unwinding ac-

tivity in the presence of 5 mM ATP. Taking a hint from the ATPase assay data, we repeated unwinding experiments at higher ATP concentrations (10 mM). The enzyme indeed efficiently unwinds the forked substrate in the presence of 10 mM ATP and complete unwinding was observed at 15 nM RECQ1[T1,helix4A] (Figure 8B, right panel). In an attempt to better understand the enzyme functioning with respect to ATP and DNA binding, we measured DNA binding affinities of RECQ1[T1] and RECQ1[T1,helix4A] using fluorescence anisotropy titrations in the presence of non-
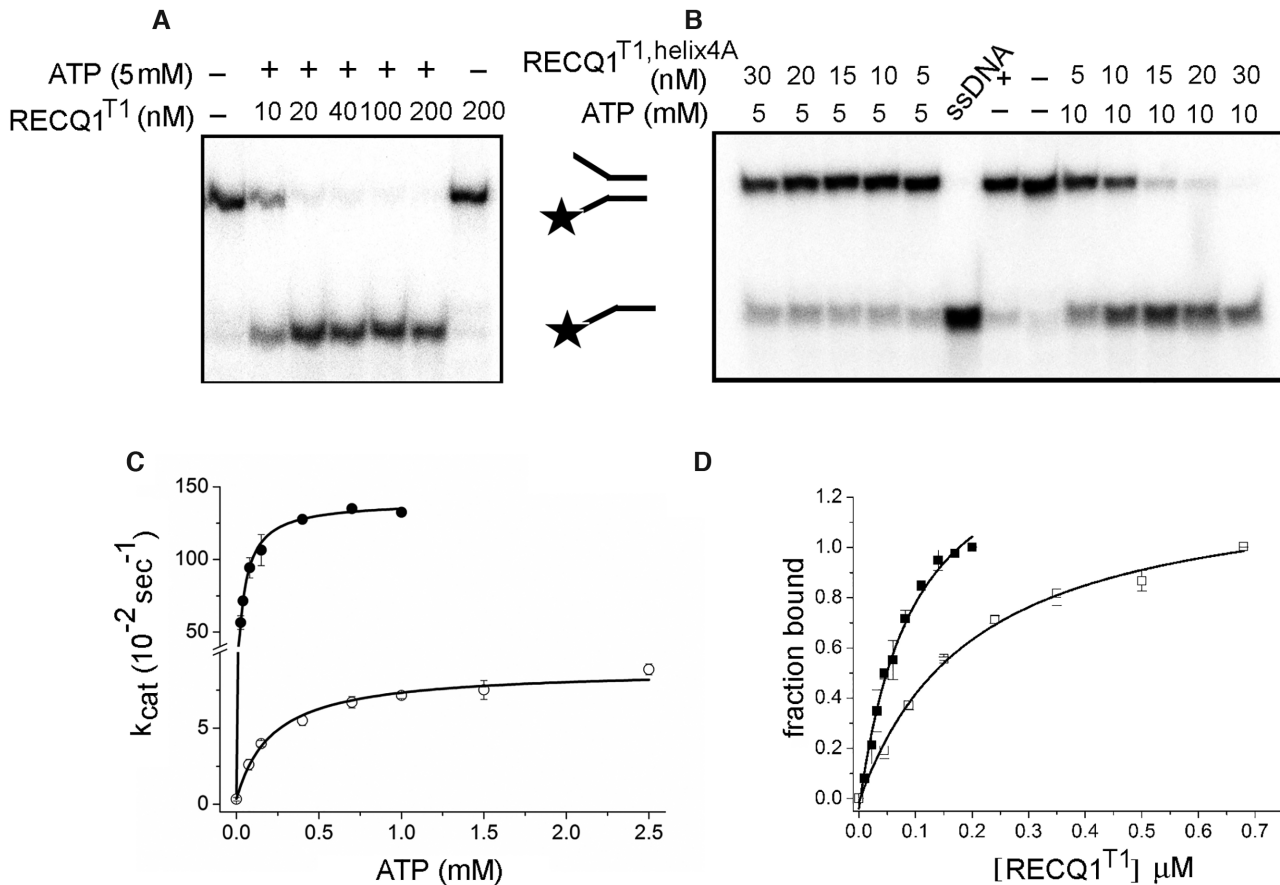
Figure 8. Unwinding and ATPase assays of RECQ1^{T1} and its mutant. (**A**) DNA unwinding assays using increasing concentrations of RECQ1^{T1} (10–200 nM) in the presence of 1 nM of ^{32}P-labelled forked duplex DNA. (**B**) DNA unwinding assays using varying concentrations of RECQ1^{T1,helix4A} (5–30 nM) in the presence of 1 nM of ^{32}P-labelled forked duplex DNA. Reactions were carried out at 37°C for 30 min in the presence of 5 mM or 10 mM ATP. Reaction carried out in the absence of ATP containing the highest concentration of enzyme (200 nM RECQ1^{T1} or 30 nM RECQ1^{T1,helix4A}) did not show any unwinding (lane adjacent to ssDNA). Products were resolved on a 12% non-denaturing PAGE and visualised using phorphorimaging. (**C**) Steady-state ATP hydrolysis assay was performed for RECQ1^{T1} (●) and RECQ1^{T1,helix4A} (○) as a function of ATP concentration in the presence of forked duplex DNA. ATPase assays were performed in presence of 0.25 μM (for RECQ1^{T1}), and 0.4 μM (for RECQ1^{T1,helix4A}) forked duplex DNA. Initial velocities were calculated from the decrease in absorbance of NADH with time and were converted to k_{cat} values. Data were fitted using Michaelis–Menten equation and $K_{M,ATP}$ values were calculated. Data shown here are the mean of at least three independent experiments, and error bars indicate standard deviation. (**D**) Measurement of DNA binding using fluorescence anisotropy titrations for RECQ1^{T1} (■) and RECQ1^{T1,helix4A} (□) were carried out with 10 nM forked duplex substrate labelled with 5′ 6-FAM in the presence of 5 mM ADPNP. The anisotropy values were converted to fraction of DNA bound, and the data were fitted using Equation (2) as mentioned in Materials and Methods and dissociation constants (K_d) were calculated. For all titrations, the data shown here are the mean of at least three independent experiments and error bars represent standard deviation.

hydrolyzable ATP analogue ADPNP (Figure 8D). The mutant (RECQ1^{T1,helix4A}) exhibits >2-fold reduction of DNA binding ($K_d = 193 \pm 27$ nM) as compared to RECQ1^{T1} ($K_d = 87 \pm 16$ nM), thereby supporting the findings from ATPase assays. Summing up the results of ATP hydrolysis and DNA binding experiments, it can be inferred that mutations on the α-helix have severely affected the coupling of DNA binding to ATP binding leading to slower ATP hydrolysis and reduced unwinding. Overall, the results from annealing, unwinding and ATPase experiments strongly support the hypothesis that mutations on the α-helix in the Zn domain might have led to the weakening of the interface resulting in impaired inter-domain communication and subsequent weakening of ATP and DNA binding.

To validate our findings in the context of the full-length RECQ1, we compared the unwinding activity of the

full-length mutant RECQ1^{FLhelix4A} with that of wild type RECQ1^{FL} (Supplementary Figure S5). The same mutations on the full-length enzyme also resulted in a weakening of unwinding activity in the presence of 5 mM ATP. While the wild type RECQ1^{FL} exhibits almost 90% unwinding starting from 5 nM enzyme, the mutant RECQ1^{FLhelix4A} can unwind only 50% substrate at 5 nM concentration and 80% at 50 nM concentration. This clearly indicates that the mutations on α-helix also affects the unwinding activity of the full-length RECQ1, although it still retains unwinding in the presence of 5 mM ATP, unlike RECQ1^{T1,helix4A}. This difference in the observed effects for the full-length and near full-length RECQ1 mutants can be attributed to the differences in the oligomeric state of the enzymes. Since the full-length RECQ1 exists in different oligomeric forms, a linear extrapolation of the findings from RECQ1^{T1} and RECQ1^{T1,helix4A} might not be reasonable.

Table 4. Summary of the strand annealing activity of human RECQ1 constructs

Name of construct	Description	Strand annealing
RECQ1^{FL}	Full-length human RECQ1	Yes[a]
RECQ1^{T1}	Truncated RECQ1 lacking 48 aa from N-terminal and 33 aa from C-terminal	No[a]
RECQ1$^{T1\Delta2Y564A}$	β-hairpin mutant of RECQ1^{T1}	Yes[a]
WH	Winged helix domain of RECQ1	Yes[a]
WH$^{\Delta2Y564A}$	β-hairpin mutant of Winged helix domain of RECQ1	Yes
D2–Zn–WH	Truncated mutant of RECQ1 encompassing D2, Zn binding domain and WH domain	No[a]
D2-Zn-CT	Truncated mutant of RECQ1 encompassing D2, Zn binding domain and WH domain till C-terminus	No
D2–Zn–WH$^{\Delta2Y564A}$	β-hairpin mutant of D2–Zn–WH	Yes
D2-Zn-CT$^{\Delta2Y564A}$	β-hairpin mutant of D2-Zn-CT	Yes
D2–Zn–WH$^{\Delta helix}$	Mutant of D2–Zn–WH lacking the α-helix (aa 420–430) in the Zn- binding domain	Yes
D2–Zn–WH^{helix4A}	Mutant of D2–Zn–WH harboring the mutation F420A, F424A, S427A, S428A on the α-helix.	Yes
RECQ1^{T1,helix4A}	Mutant of RECQ1^{T1}harboring the mutation F420A, F424A, S427A, S428A on the α-helix.	Yes
RECQ1^{FLhelix4A}	Mutant of full-length human RECQ1 harboring the mutation F420A, F424A, S427A, S428A on the α-helix	Yes

[a]Taken from Pike *et al*. and Pike *et al*. (11,15).

DISCUSSION

RECQ1 is the shortest of the five RecQ helicases identified in human comprising the conserved RecA domains (D1 and D2) and the signature RecQ C-terminal domain. Unlike other RecQ helicases, RECQ1 lacks the extended N or C terminal domains or the HRDC domain, thus making it a suitable model for studying unwinding and annealing mechanisms of RecQ family proteins. Although the mechanisms and substrate requirement for DNA unwinding by RECQ1 has been extensively studied, there is still some lack of understanding in the strand annealing mechanism. The crystal structure of a near full-length functional RECQ1 (RECQ1^{T1}) in the presence of ATPγS revealed the presence of a β-hairpin containing a tyrosine at the tip (Y564) in the WH domain that functions as a strand separation pin. Although the mutant RECQ1^{T1} retains the unwinding activity, it completely lacks the annealing activity. Mutations on the β-hairpin led to a loss of unwinding, but the same mutations restored strand annealing activity of the near full-length RECQ1^{T1}(15,16). Apparently, this restoration of annealing might have resulted as a consequence of the defect in strand separation. It was proposed that protein oligomerization might play a role in orienting the tip of β-hairpin (Y564) to create a conformation suitable for strand annealing. Pike and co-workers (2015) reported that the isolated WH domain of RECQ1 can perform strand annealing similar to the full-length enzyme, while a bigger fragment comprising D2–Zn and WH domains lacks annealing activity completely (15). The strand annealing activities of all RECQ1 mutants reported by Pike *et al*. as well as those studied by us are listed in Table 4. A careful analysis of these earlier findings prompted us to speculate that the conformation of the WH domain with respect to the rest of the protein plays a crucial role in strand annealing activity. It is possible that the restoration of strand annealing of RECQ1^{T1} upon β-hairpin mutation observed by Pike *et al*. was actually due to a conformational change in the RQC domain

leading to an altered WH domain orientation that favoured strand annealing. We, therefore, chose to dissect the mechanism of strand annealing by introducing the same mutations (Δ2Y564A on β-hairpin) in the smallest fragment of RECQ1 that lacks annealing activity (D2–Zn–WH). Mutations on β-hairpin indeed restored strand annealing activity of D2–Zn–WH, indicating that restoration of strand annealing is not just a consequence of a defect in strand separation. This notion was further strengthened by the finding that the same β-hairpin mutations, when introduced in the isolated WH domain, the mutant WH$^{\Delta2Y564A}$, exhibited a similar degree of strand annealing activity. These data clearly nullifies two possibilities; firstly, a gain of annealing is a consequence of loss in unwinding and secondly, the β-hairpin is directly contributing to the strand annealing activity. This further strengthens the speculation that the orientation of the WH domain is important for strand annealing activity.

The immediate questions that needed to be addressed were; what restricts the WH domain to achieve the favourable conformation in D2–Zn–WH or RECQ1^{T1}, and how such conformational changes are actually favoured in case of the β-hairpin mutants. We crystallized the D2–Zn–WH harbouring mutations in β-hairpin (D2–Zn–WH$^{\Delta2Y564A}$). Our crystal structure data revealed a shortened β-hairpin with significant distortions, leading to disruption or weakening of some interactions that proved to be vital for explaining the observations from strand annealing experiments. Comparing the wild type and mutant structures, we identified that the WH domain residues Y559, I567 and S568 moved away from the Zn domain, thereby weakening their interactions with F424, S427, S428 and V431 on the Zn domain. Further analysis of the interface between Zn and WH domains revealed that residues F420, F424, S427 and S428 located on an α-helix in the Zn domain significantly interact with the residues on the WH domain (Table 2). We, therefore, hypothesized that these interactions might

stabilize the interface and restrict the movement of the WH domain, thereby attenuating strand annealing activity in the constructs D2–Zn–WH or RECQ1^{T1}. Interestingly, our results indicate that deletion of the entire α-helix (D2–Zn–WH^{Δhelix}) or mutating the four residues (F420, F424, S427 and S428) to alanine (D2–Zn–WH^{helix4A}) led to the restoration of strand annealing. A precise comparison of strand annealing activities of these mutants with that of isolated WH domain revealed that D2–Zn–WH^{helix4A} exhibits similar annealing efficiency as that of WH while the mutant D2–Zn–WH^{Δhelix} can anneal even more efficiently.

In an attempt to understand the contribution of DNA binding in strand annealing activity, we assessed the binding affinities of the mutants for ssDNA and dsDNA substrates. A 1.5-fold decrease in dsDNA (blunt) and 3′ tailed duplex binding was observed for β-hairpin mutant D2–Zn–WH^{Δ2Y564A} compared to the D2–Zn–WH. The ssDNA binding for both the mutants remains almost similar. In contrast, a more significant loss in DNA binding was observed in the case of D2–Zn–WH^{helix4A}, both for blunt duplex (1.8-fold as compared to D2–Zn–WH) and 3′ tailed substrates (3-fold as compared to D2–Zn–WH). The results from our DNA binding experiments apparently indicate an inverse relationship between DNA affinities and strand annealing. Crystal structure of RECQ1^{T1} with a 3′ tailed duplex (15) demonstrated a trajectory of the DNA extended across D1, D2 and the WH domains. The double-stranded region was shown to bind primarily with the WH domain, while the single-stranded tail makes extensive contacts with the D2 domain and some contacts with the D1 domain at the 3′ end. Although a bit speculative, it is possible that mutation on the α-helix in Zn domain leads to destabilization of the interface, thereby imparting more flexibility to the WH domain and hence allowing it to orient away from the Zn domain in a conformation suitable for strand annealing. It is possible that this orientation of the WH is not allowing the contacts of WH and D2 domains with the DNA backbone and hence, not favouring the DNA binding trajectory. The reduction in DNA binding can therefore be directly correlated to the re-orientation of the WH domain, which in turn is responsible for gain in strand annealing. Therefore, our DNA binding data indirectly support the hypothesis that disruption of the interactions at the interface induces conformational changes leading to reorientation of the WH domain that favours strand annealing.

In order to strengthen our hypothesis and extrapolate our results in the context of near full-length annealing incompetent enzyme RECQ1^{T1}, we introduced the same mutations (F420A, F424A, S427A and S428A) on RECQ1^{T1}. In line with our earlier findings, the mutant RECQ1^{T1,helix4A} also exhibited efficient strand annealing of blunt and forked DNA substrates. Compared to the isolated WH domain, the mutant RECQ1^{T1,helix4A} turned out to be more efficient in annealing reactions. The increased annealing activity of RECQ1^{T1,helix4A} mutant was efficiently inhibited in the presence of human RPA70^{ΔC}, indicating that the improved annealing observed is indeed due to increased enzymatic activity. ATP binding is known to inhibit the strand annealing activity of RECQ helicases (17). Strand annealing activity of RECQ1 was reported to be significantly inhibited in the presence of 2 mM ATP and ATPγS (17).

In contrast, the annealing activity of RECQ1^{T1,helix4A} was not significantly affected in the presence of 2 mM ATP, ADP or ADPNP, but was efficiently inhibited in the presence of 5 mM ATP or ADPNP. Thus mutations on the α-helix may have rendered the protein less responsive to ATP induced conformational change. Limited proteolysis experiments with RECQ1^{T1} and RECQ1^{T1,helix4A} indicated a clear difference in digestion patterns in the presence of nucleotides. Similar to earlier report (11), proteolysis resistant bands were observed at 40 and 30 kDa for RECQ1^{T1} in the presence of nucleotides. In contrast, no distinct bands were observed at the said position in the case of RECQ1^{T1,helix4A} in the presence or absence of nucleotides. Comparison of results from limited proteolysis clearly indicates that the mutant RECQ1^{T1,helix4A} assumes a different conformation altogether that is more prone to proteolytic digestion. These results directly support our hypothesis that there is a major conformational difference in the RQC domain of the annealing incompetent RECQ1^{T1} and that of the annealing competent RECQ1^{T1,helix4A}.

DNA and ATP binding is known to act as the trigger to switch between unwinding and annealing activities (14). Surprisingly, the mutant RECQ1^{T1,helix4A} exhibits very slow DNA stimulated ATP hydrolysis kinetics and reduced affinity for ATP as compared to RECQ1^{T1}. This is interesting, particularly because the residues mutated on the α-helix are not known to be directly involved in DNA or ATP binding. Very weak unwinding was observed for RECQ1^{T1,helix4A} in the presence of 5 mM ATP and unwinding was restored in the presence of 10 mM ATP. These findings clearly demonstrate that the mutant RECQ1^{T1,helix4A} is less responsive to ATP induced conformational changes and therefore requires higher ATP concentration to achieve a conformation that favours unwinding. A >2-fold reduction in DNA binding affinity of RECQ1^{T1,helix4A} (193 nM compared to 87 nM for RECQ1^{T1}) in the presence of non-hydrolysable ATP analogue ADPNP, further confirmed that RECQ1^{T1,helix4A} is defective in coupling DNA binding to ATP binding and hydrolysis. Moreover, results from limited proteolysis experiments argue in favour of altered conformation of the RQC domain that can explain the weakening of inter-domain communication and subsequent weakening of ATP hydrolysis and unwinding.

Pike *et al.* reported a loss of unwinding and restoration of strand annealing activities due to mutations on the tip of the β-hairpin (15). Sami *et al.* have recently reported that mutation of three out of four conserved cysteine residues in the Zn domain leads to loss of ATP hydrolysis and unwinding activities and concomitant improvement of annealing activity of RECQ1 (35). In contrast to the previously reported mutants (β-hairpin mutant or Zn binding cysteine mutants), the mutations on the α-helix restore strand annealing activity of RECQ1^{T1} and at the same time retain the unwinding activity. Interestingly, in case of the mutant RECQ1^{T1,helix4A}, the residues (F420, F424, S427 and S428) are not known to have direct interaction with either Zinc or DNA or ATP. Therefore, the effects observed for the mutant RECQ1^{T1,helix4A} may be attributed to impaired inter-domain communication resulting from the destabilization of the interface. Results from

the near full-length RECQ1 mutant further enriched our hypothesis that disruption of the interface between Zn and WH domain orients the WH domain in a conformation that disfavours DNA binding, weakens inter-domain co-ordination and favours strand annealing activity. A crystal structure reported for *Cronobacter sakazakii* RecQ helicase core demonstrated DNA induced conformational change of WH domain as the key mechanism of unwinding (36). Superimposition of the *E.coli* RecQ and human RECQ1 also shows that the WH domain in *E. coli* RecQ is positioned perpendicular to the D1–D2 domains as opposed to human RECQ1, where the WH domain lies beneath the helical hairpin of ZND (11,12). A similar conformational rearrangement of the WH domain might be relevant for the strand annealing activity of human RECQ1.

To validate our findings in the context of full-length RECQ1, we introduced the same mutations (F420A, F424A, S427A and S428A) in RECQ1^{FL}. The mutant RECQ1^{FLhelix4A} also exhibits improved strand annealing and reduced unwinding activities compared to RECQ1^{FL}. Annealing of the forked substrate was observed at much lower concentrations of the mutant RECQ1^{FLhelix4A} than that of RECQ1^{FL}. Since the full-length RECQ1 is already annealing competent, improvement of strand annealing due to the mutations indicates a clear functional difference of the mutant from the wild-type. Since the full-length enzyme exists in higher oligomeric forms, a linear extrapolation of results obtained for the smaller constructs or RECQ1^{T1} might not be reasonable. However, the clear difference in annealing and unwinding activities of the full-length mutant further validates our hypothesis that conformational change in RQC resulting in altered WH orientation is required for strand annealing. A more careful and detailed investigation of the full-length mutant would be required to a get better understanding of how such conformational change is achieved in the context of full-length enzyme.

Muzzollini *et al.* demonstrated that higher-order oligomers of RECQ1 are responsible for strand annealing activity, and ATP binding is the key factor that controls the switch between strand annealing and unwinding activities. Although we do not deviate much from this hypothesis, the present study significantly adds to our current understanding of strand annealing mechanism in the context of RECQ1 monomers in particular. All the annealing competent constructs used in our study are monomeric except for the full-length enzyme. Increased annealing activity of the monomeric constructs upon mutations at the interface clearly indicates that the WH domain conformation in these monomeric mutants mimics the conformation that favours annealing in higher-order oligomers. We can speculate that in RECQ1 monomers and lower-order oligomers, the WH domain contacts the Zn domain and hence is restricted in a conformation not suitable for strand annealing. It is possible that in higher-order oligomers, the WH domain moves away from the Zn domain and exist in a different conformation stabilized by intermolecular interfaces formed between the monomer or the dimer units. The crystal structure data and mutational studies presented in this paper have improved our overall understanding of the strand annealing mechanism of human RECQ1.

The biological function of strand annealing activity of RecQ helicases, including RECQ1, remains poorly understood. RECQ1 deficiency in human cells has been shown to result in increased sensitivity to ionizing radiations (IR) or topoisomerase inhibitor like camptothecin (CPT). This in turn, leads to spontaneous γ-H2AX foci formation and elevated sister chromatid exchange indicating impairment in DNA repair (37). Moreover, RECQ1 has been shown to participate in the restoration of regressed replication forks following CPT induced DNA damage (10). Evidence from earlier studies suggests that RecQ helicases like BLM and WRN co-ordinate their annealing and unwinding activities to catalyze strand exchange reaction and promote replication fork regression (38–40). It is possible that co-ordination of the unwinding and annealing activities of RECQ1 is required for branch migration on Holliday junctions or chicken foot structures facilitating the restoration of stalled forks. A validation of this model *in vivo* might be possible using full-length or near full-length RECQ1 mutants that partly or fully lacks the unwinding but retains the annealing function. In this study, we identified the mutants RECQ1^{T1,helix4A} and RECQ1^{FLhelix4A} that have reduced unwinding and improved strand annealing activity. Genetic complementation with these mutants in RECQ1 depleted cells and assessing its effects on DNA damage response or replication stress response following treatment with DNA damaging agents might provide novel insight into the biological significance of strand annealing activity of RECQ1.

DATA AVAILABILITY

The coordinates and structure factors for the structure of D2–Zn–WH^{Δ2Y564A} have been deposited in the Protein Data Bank (PDB ID: 6JTZ).

SUPPLEMENTARY DATA

Supplementary Data are available at NAR Online.

REFERENCES

1. Croteau,D.L., Popuri,V., Opresko,P.L. and Bohr,V.A. (2014) Human RecQ helicases in DNA repair, recombination, and replication. *Annu. Rev. Biochem.*, **83**, 519–552.

2. Larsen,N.B. and Hickson,I.D. (2013) RecQ helicases: conserved guardians of genomic integrity. *Adv. Exp. Med. Biol.*, **767**, 161–184.
3. Bohr,V.A. (2008) Rising from the RecQ-age: the role of human RecQ helicases in genome maintenance. *Trends Biochem. Sci.*, **33**, 609–620.
4. Cui,S., Klima,R., Ochem,A., Arosio,D., Falaschi,A. and Vindigni,A. (2003) Characterization of the DNA-unwinding activity of human RECQ1, a helicase specifically stimulated by human replication protein A. *J. Biol. Chem.*, **278**, 1424–1432.
5. Cui,S., Arosio,D., Doherty,K.M., Brosh,R.M. Jr, Falaschi,A. and Vindigni,A. (2004) Analysis of the unwinding activity of the dimeric RECQ1 helicase in the presence of human replication protein A. *Nucleic Acids Res.*, **32**, 2158–2170.
6. Cybulski,C., Carrot-Zhang,J., Kluźniak,W., Rivera,B., Kashyap,A., Wokołorczyk,D., Giroux,S., Nadaf,J., Hamel,N., Zhang,S. *et al.* (2015) Germline RECQL mutations are associated with breast cancer susceptibility. *Nat. Genet.*, **47**, 643–646.
7. Sun,J., Wang,Y., Xia,Y., Xu,Y., Ouyang,T., Li,J., Wang,T., Fan,Z., Fan,T., Lin,B. *et al.* (2015) Mutations in RECQL gene are associated with predisposition to breast cancer. *PLoS Genet.*, **11**, e1005228.
8. Akbari,M.R. and Cybulski,C. (2015) RECQL: a DNA helicase in breast cancer. *Oncotarget*, **6**, 26558–26559.
9. Brosh,R.M. Jr (2013) DNA helicases involved in DNA repair and their roles in cancer. *Nat. Rev. Cancer*, **13**, 542–558.
10. Berti,M., Ray Chaudhuri,A., Thangavel,S., Gomathinayagam,S., Kenig,S., Vujanovic,M., Odreman,F., Glatter,T., Graziano,S., Mendoza-Maldonado,R. *et al.* (2013) Human RECQ1 promotes restart of replication forks reversed by DNA topoisomerase I inhibition. *Nat. Struct. Mol. Biol.*, **20**, 347–354.
11. Pike,A., Shrestha,B., Popuri,V., Burgess-Brown,N., Muzzolini,L., Costantini,S., Vindini,A. and Gileadi,O. (2009) Structure of the human RECQ1 helicase reveals a putative strand-separation pin. *Proc. Natl. Acad. Sci. U.S.A.*, **106**, 1039–1044.
12. Bernstein,D.A., Zittel,M.C. and Keck,J.L. (2003) High-resolution structure of the *E. coli* RecQ helicase catalytic core. *EMBO J.*, **22**, 4910–4921.
13. Popuri,V., Bachrati,C.Z., Muzzolini,L., Mosedale,G., Costantini,S., Giacomini,E., Hickson,I.D. and Vindigni,A. (2008) The human RecQ helicases, BLM and RECQ1, display distinct DNA substrate specificities. *J. Biol. Chem.*, **283**, 17766–17776.
14. Muzzolini,L., Beuron,F., Patwardhan,A., Popuri,V., Cui,S., Niccolini,B., Rappas,M., Freemont,P.S. and Vindigni,A. (2007) Different quaternary structures of human RECQ1 are associated with its dual enzymatic activity. *PLoS Biol.*, **5**, e20.
15. Pike,A.C., Gomathinayagam,S., Swuec,P., Berti,M., Zhang,Y., Schnecke,C., Marino,F., von Delft,F., Renault,L., Costa,A. *et al.* (2015) Human RECQ1 helicase-driven DNA unwinding, annealing, and branch migration: insights from DNA complex structures. *Proc. Natl. Acad. Sci. U.S.A.*, **112**, 4286–4291.
16. Lucic,B., Zhang,Y., King,O., Mendoza-Maldonado,R., Berti,M., Niesen,F.H., Burgess-Brown,N.A., Pike,A.C., Cooper,C.D., Gileadi,O. *et al.* (2011) A prominent β-hairpin structure in the winged-helix domain of RECQ1 is required for DNA unwinding and oligomer formation. *Nucleic Acids Res.*, **39**, 1703–1717.
17. Sharma,S., Sommers,J.A., Choudhary,S., Faulkner,J.K., Cui,S., Andreoli,L., Muzzolini,L., Vindigni,A. and Brosh,R.M. Jr (2005) Biochemical analysis of the DNA unwinding and strand annealing activities catalyzed by human RECQ1. *J Biol. Chem.*, **280**, 28072–28084.
18. Cheok,C.F., Wu,L., Garcia,P.L., Janscak,P. and Hickson,I.D. (2005) The Bloom's syndrome helicase promotes the annealing of complementary single-stranded DNA. *Nucleic Acids Res.*, **33**, 3932–3941.
19. Wu,L. and Hickson,I.D. (2003) The Bloom's syndrome helicase suppresses crossing over during homologous recombination. *Nature*, **426**, 870–874.
20. Wu,L., Chan,K.L., Ralf,C., Bernstein,D.A., Garcia,P.L., Bohr,V.A., Vindigni,A., Janscak,P., Keck,J.L. and Hickson,I.D. (2005) The HRDC domain of BLM is required for the dissolution of double Holliday junctions. *EMBO J.*, **24**, 2679–2687.
21. Kabsch,W. (1993) Automatic processing of rotation diffraction data from crystals of initially unknown symmetry and cell constants. *J. Appl. Cryst.*, **26**, 795–800.
22. Evans,P. (2006) Scaling and assessment of data quality. *Acta Crystallogr. D. Biol. Crystallogr.*, **62**, 72–82.
23. McCoy,A.J., Grosse-Kunstleve,R.W., Adams,P.D., Winn,M.D., Storoni,L.C. and Read,R.J. (2007) Phaser crystallographic software. *J. Appl. Cryst.*, **40**, 658–674.
24. Adams,P.D., Afonine,P.V., Bunkóczi,G., Chen,V.B., Davis,I.W., Echols,N., Headd,J.J., Hung,L.W., Kapral,G.J., Grosse-Kunstleve,R.W. *et al.* (2010) PHENIX: a comprehensive Python-based system for macromolecular structure solution. *Acta Crystallogr. D Biol. Crystallogr.*, **66**, 213–221.
25. Emsley,P. and Cowtan,K. (2004) Coot: model-building tools for molecular graphics. *Acta Crystallogr. D. Biol. Crystallogr.*, **60**, 2126–2132.
26. Lee,B. and Richards,F.M. (1971) Interpretation of protein structures-estimation of static accessibility. *J. Mol. Biol.*, **55**, 379–400.
27. Hubbard,S.J. and Thornton,J.M. (1993) Naccess. In: *Computer Program, Department of Biochemistry and Molecular Biology*. University College London, UK.
28. Schneider,C.A., Rasband,W.S. and Eliceiri,K.W. (2012) NIH image to Image J: 25 years of image analysis. *Nat. Methods*, **9**, 671–675.
29. Ganguly,A., del Toro Duany,Y., Rudolph,M.G. and Klostermeier,D. (2011) The latch modulates nucleotide and DNA binding to the helicase-like domain of *Thermotoga maritima* reverse gyrase and is required for positive DNA supercoiling. *Nucleic Acids Res.*, **39**, 1789–1800.
30. Ganguly,A., del Toro Duany,Y. and Klostermeier,D. (2013) Reverse gyrase transiently unwinds double-stranded DNA in an ATP-dependent reaction. *J. Mol. Biol.*, **425**, 32–40.
31. Jones,S., Marin,A. and Thornton,J.M. (2000) Protein domain interfaces: characterization and comparison with oligomeric protein interfaces. *Protein. Eng.*, **13**, 77–82.
32. Jones,S and Thornton,J.M. (1996) Principles of protein-protein interactions. *Proc. Natl. Acad. Sci. U.S.A.*, **93**, 13–20.
33. Gomes,X.V. and Wold,M.S. (1996) Functional domains of the 70-Kilodalton subunit of human replication protein A. *Biochemistry*, **35**, 10558–10568.
34. Shen,J.C., Lao,Y., Kamath-Loeb,A., Wold,M.S. and Loeb,L.A. (2003) The N-terminal domain of the large subunit of human replication protein A binds to Werner syndrome protein and stimulates helicase activity. *Mech. Ageing Dev.*, **124**, 921–930.
35. Sami,F., Gary,R.K., Fang,Y. and Sharma,S. (2016) Site-directed mutants of human RECQ1 reveal functional importance of the zinc binding domain. *Mutat. Res.*, **790**, 8–18.
36. Manthei,K.A., Hill,M.C., Burke,J.E., Butcher,S.E. and Keck,J.L. (2015) Structural mechanisms of DNA binding and unwinding in bacterial RecQ helicases. *Proc. Natl. Acad. Sci. U.S.A.*, **112**, 4292–4297.
37. Sharma,S. and Brosh,R.M. Jr (2007) Human RECQ1 is a DNA damage responsive protein required for genotoxic stress resistance and suppression of sister chromatid exchanges. *PLoS One*, **2**, e1297.
38. Wu,Y. (2012) Unwinding and rewinding: double faces of helicase? *J. Nucleic Acids*, **2012**, 140601.
39. Machwe,A., Xiao,L., Groden,J., Matson,S.W. and Orren,D.K. (2005) RecQ family members combine strand pairing and unwinding activities to catalyze strand exchange. *J. Biol. Chem.*, **280**, 23397–23407.
40. Machwe,A., Xiao,L., Lloyd,R.G., Bolt,E. and Orren,D.K. (2007) Replication fork regression in vitro by the Werner syndrome protein (WRN): holliday junction formation, the effect of leading arm structure and a potential role for WRN exonuclease activity. *Nucleic Acids Res.*, **35**, 5729–5747.